Contrib Mineral Petrol (2006) 152:223–242
DOI 10.1007/s00410-006-0106-3

ORIGINAL PAPER

Geochronological constraints on the Legs Lake shear zone with implications for regional exhumation of lower continental crust, western Churchill Province, Canadian Shield

K. H. Mahan · M. L. Williams · R. M. Flowers · M. J. Jercinovic · J. A. Baldwin · S. A. Bowring

Received: 22 August 2005 / Accepted: 1 May 2006 / Published online: 14 June 2006

Abstract The Legs Lake shear zone marks the southeastern boundary of an extensive region (>20,000 km^2) of high-pressure (0.8–1.5+ GPa) granulite-facies rocks in the western Churchill Province, Canada. The shear zone is one of the largest exhumation-related structures in the Canadian Shield and coincides with the central segment of the ~2,800 km long Snowbird tectonic zone. The movement history of this shear zone is critical for the development of models for the exhumation history of the high-pressure region. We used electron microprobe U–Th–Pb dating of monazite with supplemental ID-TIMS U–Pb geochronology to place constraints on the timing of shear zone activity. Combining these and other data, we suggest that regional exhumation occurred during at least three distinct phases over an ~150 million year period. The first phase involved high temperature decompression from ~1.0 to 0.8–0.7 GPa shortly following 1.9 Ga peak metamorphism, possibly under an extensional regime. The second phase involved rock uplift and decompression of the hanging wall to 0.5–0.4 GPa during east-vergent thrusting across the Legs Lake shear zone at ca. 1.85 Ga. This phase was likely driven by early collision-related convergence in the Trans-Hudson orogen. The final phase of regional exhumation, involving the removal of 15–20 km of overburden from both footwall and hanging wall, likely occurred after ~1.78 Ga and may have been related to regional extensional faulting.

Electronic Supplementary Material Supplementary material is available to authorised users in the online version of this article at http://dx.doi.org/10.1007/s00410-006-0106-3.

Communicated by T. L. Grove

K. H. Mahan · M. L. Williams · M. J. Jercinovic
Department of Geosciences,
University of Massachusetts-Amherst,
611 N. Pleasant St., Amherst, MA 01003, USA

R. M. Flowers · S. A. Bowring
Department of Earth, Athmospheric and Planetary Sciences, Massachusetts Institute of Technology, Cambridge, MA, USA

J. A. Baldwin
Department of Geology, University of Maryland, College Park, MD, USA

Present address: K. H. Mahan (✉)
Division of Geological and Planetary Sciences, California Institute of Technology, Mailstop 100-23, Pasadena, CA 91125, USA
e-mail: kmahan@gps.caltech.edu

Introduction

Exposures of lower continental crust provide rare opportunities to directly investigate a part of Earth that is generally inaccessible except by geophysical methods or sparse remote sampling by xenoliths. A critical aspect of the characterization of such terranes is to understand the mechanisms and rates by which they are exhumed (Fountain and Salisbury 1981; Handy 1990; Percival et al. 1992). The exhumation history is particularly important for understanding the tectonic setting of exposed deep crustal terranes, for evaluating the degree to which they preserve a record that is indicative of lower crustal processes in general, and for understanding the nature of the crust that is currently present beneath these terranes. As is commonly the

case in polyphase metamorphic terranes in general, distinguishing between earlier events related to initial burial and/or residence in the lower crust and those associated with exhumation can be challenging and commonly requires complimentary geochronological techniques with careful textural and spatial control (e.g., Vance et al. 2003).

A major component of the exhumation history of deep crustal terranes is commonly recorded in bounding fault zones (e.g., Fountain and Salisbury 1981; Handy 1990). Some well-known examples include the Ivanhoe fault bounding the Kapuskasing uplift in the central Canadian Shield (e.g., Percival and West 1994), the Pogallo shear zone and Insubric Line in the Ivrea Zone (e.g., Handy and Zingg 1991), the Grenville Front tectonic zone (e.g., Green et al. 1988), the Red Bank thrust zone bounding the Arunta block in central Australia (Teyssier 1985; Biermeier et al. 2003), and shear zones bounding the granulite terrane in Fiordland, New Zealand (e.g., Klepeis et al. 1999). Characterizing these structures, and in particular determining the absolute timing of their development, is critical for understanding their role in the exhumation history as well as for the development of exhumation models in general.

An extensive region (>20,000 km^2) of high-pressure (*P*) (0.8–1.5+ GPa) granulite- and locally eclogite-facies rock is exposed north and east of Lake Athabasca in the central part of the western Churchill Province (Fig. 1) (Williams and Hanmer 2005; Mahan and Williams 2005) of the Canadian Shield. The most extensively studied portion of this region is the East Athabasca mylonite triangle (Hanmer 1994, 1997; Hanmer et al. 1994; Fig. 2), and several of its most distinctive components include a major deep-crustal mafic dike swarm (Williams et al. 1995; Flowers et al. 2006a), one of the oldest (~1.9 Ga) known eclogite occurrences (Snoeyenbos et al. 1995; Baldwin et al. 2004), and a 2.6 Ga regional charnockite batholith in transition to Grt-granulite (Williams et al. 2000) (mineral abbreviations after Kretz 1983). High-*P* granulite-facies metamorphic events are recorded over much of the region at both 2.6–2.5 and 1.9 Ga with an inferred intervening period of relatively quiescent deep crustal residence (Williams and Hanmer 2005; Flowers 2005). The region is potentially one of the best exposures on Earth for the study of deep continental crustal processes, and understanding its exhumation is crucial.

The southeastern boundary of the high-*P* terrane coincides with the Snowbird tectonic zone (Goodacre et al. 1987; Hoffman 1988; Hanmer 1997) and is specifically defined by the Legs Lake shear zone. This km-scale, east vergent, thrust-sense shear zone marks a ~20 vertical km juxtaposition in the east Lake Athabasca area, and has been kinematically and temporally linked to similar along-strike structures giving a combined length of at least 500 km (Fig. 1b) (Mahan et al. 2003; Mahan and Williams 2005). High-*P* (1.0+ GPa) granulite-facies metamorphism is recorded in the hanging wall, whereas pressures recorded in the Hearne footwall reached a maximum of 0.5 GPa (Mahan et al. 2003).

Recent U/Pb ID-TIMS data demonstrate that the youngest high-*P* metamorphic event in the east Lake Athabasca area occurred at ca. 1.9 Ga (Baldwin et al. 2003, 2004; Flowers et al. 2006a), providing a

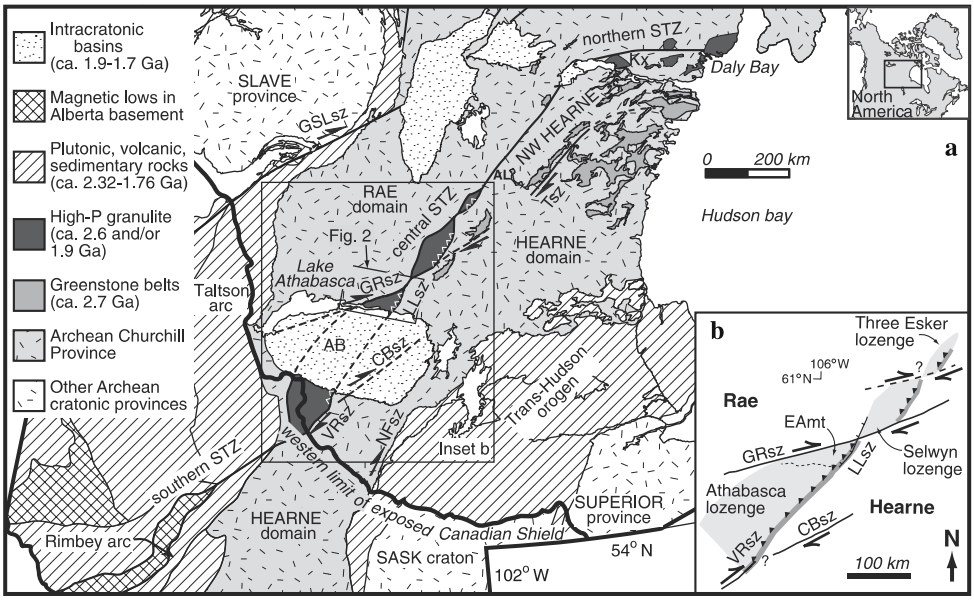

Fig. 1 **a** Western Canadian Shield. *Box* shows location of (**a**). *AB* Athabasca basin, *AL* Angikuni Lake, *Kx* Kramanituar complex, *STZ* Snowbird tectonic zone, Shear zones: *LLsz* Legs Lake, *GRsz* Grease River, *GSLsz* Great Slave Lake, *CBsz* Cable Bay, *NFsz* Needles Falls, *Tsz* Terrell, *VRsz* Virgin River. *Rectangle* shows location inset **b** and of Fig. 2. **b** *Inset* shows distribution of and relationship between major shear zones of central Snowbird tectonic zone after Mahan and Williams (2005)

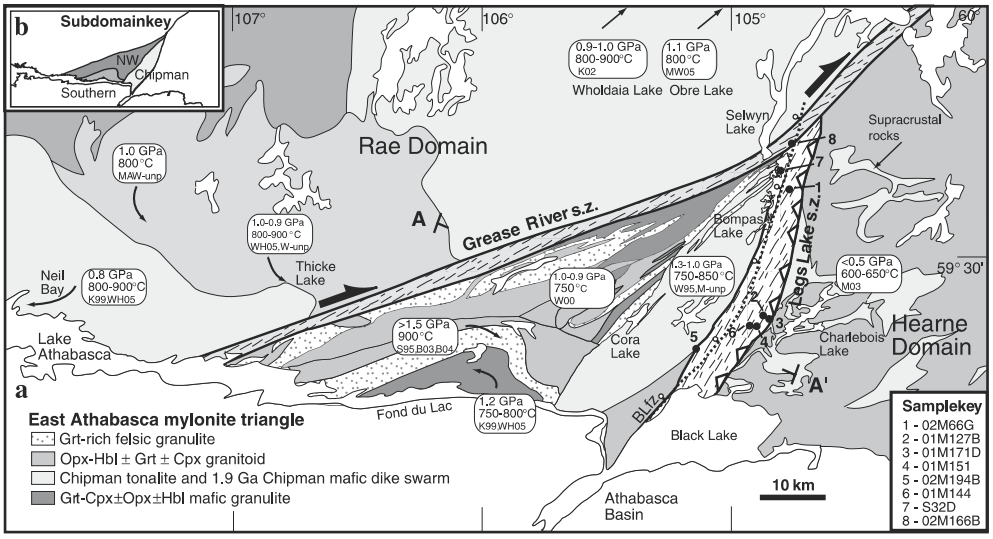

Fig. 2 **a** Geologic map of the East Athabasca mylonite triangle and surrounding Rae and Hearne domains. Subdomain boundaries within Rae domain are also shown. East Athabasca triangle geology after Hanmer (1994). References for *P–T* data: MAW-unp = Mahan, Ashton and Williams, unpublished; M-unp = Mahan, unpublished; W-unp = Williams, unpublished, S95 = Snoeyenbos et al. 1995; W95, W00 = Williams et al. 1995, 2000; K99 = Kopf 1999; K02 = Krikorian 2002; B03, 04 = Baldwin et al. 2003, 2004; M03 = Mahan et al. 2003; MW05 = Mahan and Williams 2005; WH05 = Williams and Hanmer 2005. **b** Key to lithotectonic subdomains of the East Athababasca mylonite triangle

maximum age for regional exhumation of the terrane. Exhumation was complete by 1.7 Ga, the approximate age of the overlying, undeformed and unmetamorphosed Athabasca basin (Cumming et al. 1987; Rayner et al. 2003). Within these broad limits, two endmember exhumation scenarios can be considered. Regional uplift of the terrane may have been associated with ca. 1.9 Ga deep crustal tectonometamorphic events or alternatively, exhumation may have been related to ca. 1.85–1.80 Ga collisional events recorded in the Trans-Hudson orogen to the southeast. These two models imply exhumation as either (1) an isostatic response to deep-crustal underplating and heating and/or crustal thickening recorded by high-*P* metamorphism or, (2) a response to far-field convergence and crustal shortening at a distinctly later time.

Monazite is a particularly valuable geochronometer for dating metamorphic and deformation events in complex terranes because of its propensity for growth during metamorphism (e.g., Parrish 1990; Spear and Pyle 2002), slow rates of Pb diffusion (e.g., Crowley and Ghent 1999; Cherniak et al. 2004), and tendency to incorporate very little common Pb (e.g., Parrish 1990). In addition, recent studies have begun to significantly improve our ability to link monazite to metamorphic processes (e.g., Pan 1997; Pyle and Spear 1999; Spear and Pyle 2002; Wing et al. 2003; Foster et al. 2004; Kohn and Malloy 2004; Mahan et al. 2006). In this study, we employ electron microprobe monazite dating and supplement these data with additional targeted ID-TIMS analyses from monazite and zircon to constrain the timing of Legs Lake shear zone deformation. The former technique has the advantages of in situ analysis and high spatial resolution (micron-scale) (e.g., Montel et al. 1996; Williams et al. 1999; Williams and Jercinovic 2002) and the latter provides high precision and the ability to assess accuracy through multiple independent U–Pb isotope chronometers. This combination of tools, particularly when further combined with detailed X-ray compositional mapping, provides optimal potential for directly constraining the age of deformation and metamorphic events and thus significantly improving construction of *P–T–t–D* histories.

We conclude that regional exhumation of high-*P* rocks in the east Lake Athabasca area was a multiphase process that likely involved both endmembers considered above. We suggest that major movement in the Legs Lake shear zone, and a major component of regional exhumation of the high-*P* hanging wall to the middle-crust, were coincident with ca. 1,850 Ma early collision-related events in the Trans-Hudson orogeny.

Geologic setting

More than a decade of structural, metamorphic, and geochronological studies in the east Athabasca region,

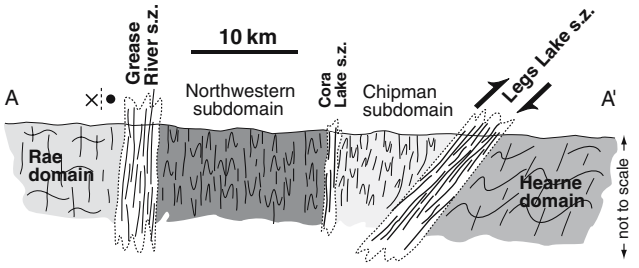

Fig. 3 Schematic NW–SE cross-section across East Athabasca mylonite triangle illustrating shear zones that form major domain and subdomain boundaries. Location shown in Fig. 2

the majority of which have been focused within the East Athabasca mylonite triangle (Figs. 2, 3), have documented two high-*P* (~1.0+ GPa) granulite-facies deformation and metamorphic events, one at ca. 2.6–2.5 Ga and one at ca. 1.9 Ga (Hanmer et al. 1994, 1995a, b; Snoeyenbos et al. 1995; Williams et al. 1995, 2000; Kopf 1999; Krikorian 2002; Baldwin et al. 2003, 2004, 2006; Flowers 2005; Flowers et al. 2006a; Williams and Hanmer 2005; Mahan et al. 2006). The degree to which these events are recorded in a particular rock or region varies among the different lithotectonic subdomains (Fig. 2b). In the northwestern subdomain, the late Archean event(s) are recorded by ca. 2.6 Ga charnockitic granitoids that display a well-defined transition to Grt-granulite that is interpreted to have developed shortly after crystallization (Williams et al. 2000). In the southern subdomain, Baldwin et al. (2003, 2004, 2006) reported 2.62–2.52 Ga monazite and zircon growth in felsic and mafic granulites. In addition, volumetrically minor lenses of high-*P* felsic and mafic granulite in the Chipman subdomain also preserve a distinct record of late Archean and ca. 1.9 Ga events (Flowers 2005; Mahan et al. 2006).

Baldwin et al. (2003, 2004) interpreted metamorphic zircon growth at 1,904 ± 0.3 Ma in mafic granulite and eclogite assemblages to record very high pressure, high temperature (1.5+ GPa, 900–1,000°C) metamorphism of southern subdomain rocks. Partial decompression and re-equilibration of these rocks to ca. 1.0 GPa apparently coincided with more widespread 1,900–1,890 Ma tectonometamorphism recorded throughout the East Athabasca region. This latter phase of metamorphism and deformation appears best recorded in the Chipman subdomain where Grt ± Cpx + Hbl + Pl + Qtz Chipman mafic dikes record partial melting at 1.1–1.0 GPa, 800°C (Williams et al. 1995) and are interpreted to have been emplaced, metamorphosed and melted at 1896.7 ± 0.8 Ma (Flowers et al. 2006a).

Late symplectite Grt ± Opx ± Hbl + Pl + Qtz assemblages recording conditions of 0.8–0.7 GPa, ~700°C, from studies in the southern (Kopf 1999) and Chipman subdomains (K.H. Mahan, unpublished data), suggest that a period of relatively rapid decompression from regional peak pressures accompanied the 1,896 Ma event. Evidence for both periods of high-grade tectonometamorphism have also been documented in other parts of the interior of the western Churchill Province (Stern and Berman 2000; Berman et al. 2002; Sanborn-Barrie et al. 2001).

The Legs Lake shear zone is a 5–8 km wide zone of northeast striking and northwest-dipping mylonite, traced along the southeastern margin of the East Athabasca triangle (Fig. 2; Mahan et al. 2001, 2003). A northward continuation of the shear zone is exposed along the eastern margin of the Selwyn lozenge to the north (Fig. 1b) and is offset dextrally from its southern counterpart across the younger Grease River shear zone (Mahan and Williams 2005). The likely correlation of these two shear zone segments with the Virgin River shear zone, south of the 1.7 Ga Athabasca basin (Fig. 1), gives a combined length on the order of 500 km and represents one of the largest fault zones in the Canadian Shield. The Legs Lake shear zone records oblique dextral reverse movement that accommodated east-vergent relative uplift (and exhumation) of high-*P* rocks in its hanging wall. The shear zone marks an abrupt juxtaposition of over 20 vertical km with low-pressure rocks in the Hearne domain to the east. Grt ± Crd ± Sil + Bt + Pl + Qtz metamorphic assemblages within and east of the shear zone record synkinematic prograde metamorphism (Fig. 4) and post-kinematic peak conditions of ~0.5 GPa and 600°C (Mahan et al. 2003). An upper bound on the age of deformation in the Legs Lake shear zone is inferred from 1.9 Ga high-*P* metamorphism in the hanging wall and shear zone-related deformation of 1.9 Ga Chipman mafic dikes.

Electron microprobe monazite geochronology

Analytical methods

The methods used for evaluating the textural setting of monazite follow those of Williams and Jercinovic (2002). All X-ray maps and wavelength-dispersive spectrometric analyses were done at the University of Massachusetts-Amherst using a Cameca SX-50 electron microprobe. The distribution of monazite was evaluated using thin section X-ray composition images of Ce (for identification of monazite) and a reference major element such as Mg (for overall texture of the thin section). High resolution composition (beam

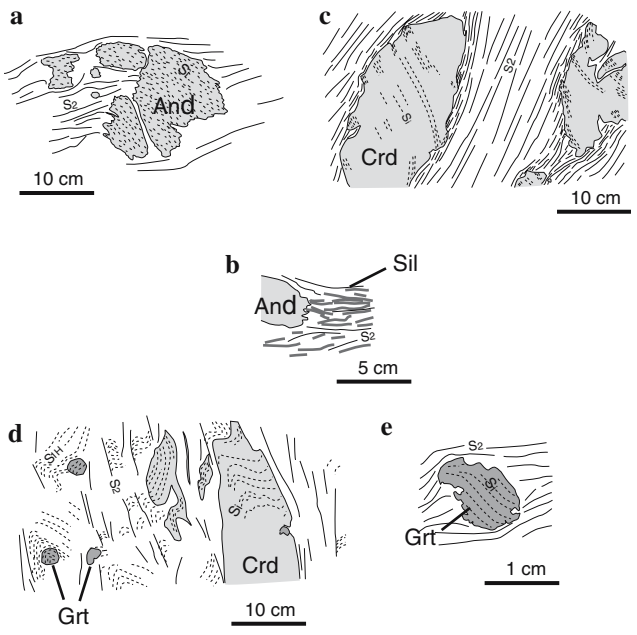

Fig. 4 Sketches from thin sections illustrating the relationships between porphyroblast growth and fabric development in Hearne domain (Mahan et al. 2003). S_i = inclusion trail fabric. S_{1H} = early matrix fabric in Hearne domain. S_{SZ} = Legs Lake shear zone fabric. Andalusite porphyroblasts generally preserve straight inclusion trail patterns, interpreted as an earlier fabric (S_i), but a slight curvature of S_i toward the matrix fabric occurs within some porphyroblast rims (**a**) indicating synkinematic growth with respect to D_{SZ}. Replacement of andalusite by prismatic and fibrous sillimanite, the latter of which is grown parallel to S_{SZ}, is also interpreted as synkinematic. **b** Cordierite occurs as both intact porphyroblasts, with curving inclusion trail patterns (**c**), as well as S_{SZ}-parallel elongate polycrystalline aggregates that are interpreted to have recrystallized during D_{SZ} in higher strain parts of the shear zone. Garnet occurs as similar, inclusion trail-bearing, synkinematic porphyroblasts (**d**, **e**) and as late- to post-kinematic porphyroblasts that lack inclusion trails

scanning) maps of Y, Th, U, and Pb and/or Ca were generated for all monazite grains in textural settings of interest.

Analytical conditions for major and trace element calibrations and for major element analyses were 15 kV accelerating voltage, 15 nA current, focused beam, and 20 s peak count time (10 s background count time). Procedures for trace element analysis, including determination of background intensities via regression of high-resolution spectrometer scans, followed Jercinovic and Williams (2005), and the approach and data presentation follow Williams et al. (2006). Spot analyses were carried out at 15 kV accelerating voltage, 200 nA beam current, and 600 s count time (900 s count times were used for domains with <1.0 wt% Th). For each homogeneous compositional domain, between 4 and 20 point analyses were obtained. Weighted mean compositions of Th, U, and Pb were then calculated based on the analytical uncertainties from counting statistics for each analysis (Table 1). A single date for that domain was then calculated from the weighted mean compositions and the age equation of Montel et al. (1996). Dates quoted in the text and in Table 1 are reported with a 2σ error, calculated by propagating the analytical uncertainty on trace element compositions and an uncertainty component associated with the background regression through the age equation (Williams et al. 2006). Microprobe dates for multiple domains are displayed graphically in the form of normal distribution curves. Weighted mean dates and 95% confidence errors for groups of 3 or more monazite domains within a sample, when interpreted to represent a single population, were calculated with the Isoplot/Ex v. 3 program of Ludwig (2003).

Analytical results

Deformed granite dikes

Muscovite leucogranite dikes (dm- to m-scale in width) occur extensively within the shear zone in a region east of Bompas Lake (Fig. 2) where they intrude metasedimentary rocks of the Hearne domain. These dikes are penetratively mylonitized and/or exhibit boudinage parallel to the shear fabric (Fig. 5a) and their crystallization age provides a maximum age for their deformation.

Monazite from sample 02M66G is not abundant in thin section, but several large (100–500 μm) grains were isolated using conventional mineral separation techniques. Five grains were mounted in epoxy and analyzed by EMP. X-ray maps of four of the grains display large compositionally homogeneous regions with rare mildly contrasting and straight compositional domain boundaries that are interpreted to represent sector zoning in igneous monazite. These grains also display small (10–30 μm wide) discontinuous rim domains (Fig. 6a, b) characterized by distinctly lower U concentration (Fig. 7a) (<0.5 wt% vs. >1.0 wt% in cores). The cores of these four grains yield microprobe dates between 2,490± 20 and 2,504±16 Ma (Fig. 6c). Rim domains yield ca. 1.9 Ga dates that are best represented by recrystallized domains in the fifth grain (below). Trace element data are presented in Table 1 and major element analyses of monazite are provided as electronic supplementary material (eTable 1).

The fifth grain (m1) displays a similar compositional variation but with considerably more complex internal zoning that suggests extensive dissolution and reprecipitation (Fig. 6d). The original high U domains,

Table 1 Monazite trace element compositions and electron microprobe dates

Gr[a]	Set[b]	Dom[c]	Concentration (ppm)[d]								*n*	Date	2σ
			Y	1σ	Th	1σ	Pb[e]	1σ	U[f]	1σ			
02M66G (UTM_N: 6611794, UTM_E: 504873)													
m1	mo	core	22,339	24	33,145	34	17,681	31	12,646	19	20	2,554	12
m2	mo	core	21,894	25	36,370	37	12,897	18	18,091	32	19	2,504	10
m3	mo	core	18,778	28	31,110	40	9,967	20	13,232	36	13	2,504	16
m4	mo	core	20,137	36	34,003	54	9,955	26	12,643	45	8	2,490	20
m5	mo	core	20,105	29	35,709	46	10,555	21	13,478	37	12	2,491	16
Population 2-recrystallized													
m1	mo	re-xtl	17,127	18	37,417	31	4,655	11	4,190	22	28	1,889	14
01M127B (UTM_N: 6586933, UTM_E: 501034)													
m1	m	wh	12,400	25	70,552	60	8,377	14	8,510	25	20	1,775	10
tm1	mo	wh	9,822	24	64,173	77	6,883	20	5,543	38	11	1,758	18
tm2	mo	core	10,970	24	72,264	85	7,871	21	6,598	39	11	1,760	16
tm2	mo	rim	6,825	36	24,477	61	3,280	28	3,992	58	4	1,804	50
tm3	mo	wh	11,307	37	69,063	121	7,975	31	7,709	57	5	1,767	24
01M171D (UTM_N: 6586196, UTM_E: 502456)													
Population 1													
1-m3	m	core	10,746	33	14,498	41	2,133	22	2,605	48	5	1,898	64
1-m7	m	core	9,619	50	19,577	56	2,827	27	3,214	59	3	1,921	62
2-m6	m, ib	wh	10,611	25	20,082	33	2,771	15	2,988	32	11	1,908	36
2-m11	m	core	11,869	38	12,760	42	1,820	24	2,075	54	4	1,909	84
2-m16	m	core	12,048	38	19,282	47	2,590	23	2,827	48	5	1,872	54
Population 2a													
1-m2	m	wh	10,995	25	24,731	42	3,361	17	3,897	37	8	1,848	32
1-m3	m	rim	13,680	30	26,509	48	3,662	21	4,432	42	7	1,837	34
1-m7	m	rim	14,616	43	27,819	57	4,210	23	5,695	48	5	1,853	32
1-m8	m	wh	11,346	29	26,167	50	3,502	20	3,977	42	6	1,844	36
1-m9	m	wh	13,328	31	26,741	51	3,845	20	4,903	43	6	1,844	32
2-m7	m, ip	wh	14,470	39	29,634	61	4,008	25	4,476	50	5	1,865	38
2-m11	m	rim	10,854	24	24,624	38	2,964	16	2,661	34	10	1,849	34
2-m13	m, ip	wh	14,797	24	27,617	36	3,989	15	5,279	31	13	1,824	22
2-m15	m	wh	12,864	38	24,845	55	3,505	24	4,364	49	5	1,841	40
2-m17	m	core	16,164	33	21,054	39	2,795	18	3,165	39	8	1,837	40
2-m20	m, ig	wh	12,008	38	25,603	56	3,540	24	4,042	48	5	1,873	42
Population 2b													
1-m1	m	wh	13,421	25	26,033	40	3,578	17	4,566	35	10	1,800	28
1-m4	m	wh	13,471	31	28,982	54	3,920	21	4,965	43	6	1,789	30
2-m3	m	wh	13,676	38	24,896	55	3,408	24	4,444	49	5	1,782	40
2-m16	m	rim	11,748	25	24,892	38	3,145	17	3,454	35	10	1,802	32
2-m17	m	rim	14,900	40	27,919	59	3,799	24	4,826	50	5	1,794	36
01M151 (UTM_N: 6585101, UTM_E: 500317)													
Population 2													
m4	m, ic, q, c	wh	11,483	27	33,158	54	4,639	19	5,724	40	7	1,834	26
m6	m, ic, q	wh	10,134	30	32,392	64	3,790	24	3,513	48	5	1,798	36
m8	m	wh	11,257	35	33,470	72	4,574	25	5,516	53	4	1,826	34
m9	m	wh	10,726	30	29,845	59	3,861	23	4,339	47	5	1,813	36
m13	m, ic, b	wh	10,871	13	22,895	41	3,261	20	4,493	23	4	1,781	35
02M194B (UTM_N: 6584847, UTM_E: 491625)													
Population 1a													
m2	m, ig	wh	7,386	33	39,621	78	7,681	31	3,366	52	4	2,967	48
m5	m, ig	wh	7,261	25	23,416	44	5,568	21	3,629	39	7	2,975	42
Population 1b													
m1	m	core	5,673	36	35,833	90	6,751	34	3,129	59	3	2,880	56
m7	m	core	5,926	10	29,275	52	6,446	29	4,136	52	4	2,885	48
m7	m	mtl	4,843	25	27,333	52	5,514	23	3,300	42	6	2,809	44
Population 2													
m9	m, ig, q	wh	4,408	28	27,039	56	5,023	24	3,588	46	5	2,556	46
m6	m	core	2,568	22	31,776	50	5,494	20	3,410	36	8	2,549	34
Population 3													
m3	m	wh	10,566	26	9,359	28	1,847	17	2,975	38	7	1,936	58

Table 1 continued

Gr[a]	Set[b]	Dom[c]	Concentration (ppm)[d]								*n*	Date	2σ
			Y	1σ	Th	1σ	Pb[e]	1σ	U[f]	1σ			
m11	m	wh	9,941	28	4,358	26	1,418	18	3,023	41	6	1,945	76
m7	m	rim	4,168	27	28,641	59	3,136	22	1,735	45	5	1,918	46
Population 4													
m4	m	wh	11,326	26	51,497	72	4,948	19	2,145	37	8	1,795	24

[a] *tm*# Analyzed in tube mount, *m* analyzed in thin section [# preceding "m" corresponds to one of two sections from same billet]

[b] *m* Matrix, *ig* inclusion in garnet (ic, cordierite; ib, biotite; ip, plagioclase), *mo* mounted separate, *c* visible fractures in adjacent host, *q* in contact with qtz inclusion, *g* interior of grt, not true inclusion, *b* in contact with bt inclusion

[c] *Wh* Whole grain, *Mtl* mantle

[d] Element lines (and crystals) used were YLα(TAP), ThMα (PET), UMβ (PET), PbMα (PET)

[e] Measured on PbMα and corrected for Y and Th interferences

[f] Measured on UMβ and corrected for Th interferences. The data were screened to avoid potential marginal K interference from adjacent phases (Jercinovic and Williams 2005)

5–50 μm wide zones similar to cores of the other four grains, form a variably interconnected network surrounded by regions of lower U (<0.5 wt%). An "age" map for this grain, generated by calculating dates for each pixel in high-resolution calibrated X-ray maps (Goncalves et al. 2005), shows dramatic variation in age that correlates well with U concentration (Fig. 6e). Interestingly, abundant apatite inclusions are restricted to the recrystallized portions of the monazite, suggesting that apatite growth may have been coeval with monazite recrystallization, similar to monazite-apatite reactions studied by Harlov et al. (2002) and Harlov and Förster (2003). The high U domains of m1 yield a date of 2,554 ± 12 Ma. A weighted mean date for the first four grains is 2,500 ± 7 Ma (MSWD = 1.05) and for all five high U domains is 2,514 ± 34 Ma (MSWD = 16). There are no significant compositional or textural variations to suggest that the high U domains are not part of one igneous population and therefore, we consider the latter date as the best estimate of the crystallization age for this rock. The low U recrystallized domains in m1 yield a significantly younger date of 1,889 ± 14 Ma.

Undeformed Grt-Ms-granite dikes

A distinct suite of post-kinematic, pink, Grt-Ms granite and pegmatite dikes occurs within the eastern margin of the Legs Lake shear zone as well as over an extensive region, outside of the shear zone, near the western end of Charlebois Lake (Fig. 2). In the shear zone, the dikes clearly cut the mylonitic fabric and these relationships can be observed in several locations (Fig. 5b, c). Therefore, the crystallization age of these dikes provides a lower constraint on the timing of shear zone deformation. Sample 01M127B is from a thin dike that cross-cuts mylonitic fabric near the eastern margin of the shear zone.

A single grain in a thin section of sample 01M127B and three grains (100–200 μm) from conventional separates were analyzed and contain 6.0–7.0 wt% Th. The monazite grains display either no compositional zonation, mild sector zoning with straight boundaries, or euhedral concentric zoning (Fig. 8a, b). The relatively simple zoning pattern and the undeformed nature of the sample suggest an igneous origin for the monazite. Three whole grains and the core of a fourth concentrically zoned grain yield dates between 1,758 ± 18 and 1,775 ± 10 Ma, whereas the rim of the fourth grain yielded 1,804 ± 50. A weighted mean of all five domains is 1,769 ± 12 Ma (MSWD = 1.5) or, if the outlying rim is excluded, 1,768 ± 14 (MSWD = 1.4) (Fig. 8c).

Metamorphic monazite from metasediments in the Hearne domain

Metasedimentary rocks occur interlayered with granodioritic gneiss and are commonly associated with layered felsic to mafic metavolcanic rocks on the southeastern side of the shear zone (Mahan et al. 2003). The most common lithology is Bt-schist with variable amounts of garnet, cordierite, andalusite, and sillimanite. Microstructural observations indicate that early andalusite, garnet, cordierite, and sillimanite growth occurred syn-kinematically during shear zone fabric development (Fig. 4) with continued post-kinematic growth of garnet and cordierite (Mahan et al. 2003).

Two samples of Bt-schist were chosen for compositional mapping and monazite dating, but the majority of data reported is from sample 01M171D. In both

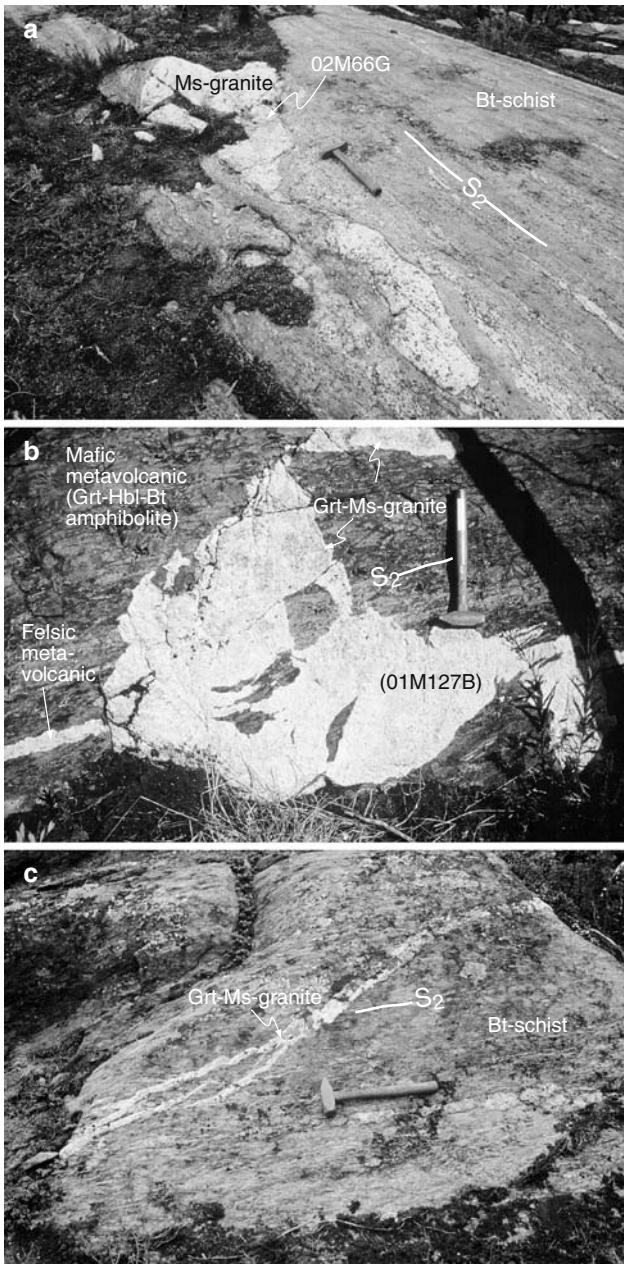

Fig. 5 **a** Outcrop photo of foliated boudins of Ms leucogranite hosted by Bt-schist in the Legs Lake shear zone east of Bompas Lake. Sample 02M66G was collected from the larger boudin left of the hammer (30 cm long). **b** Outcrop photo of post-kinematic Grt-Ms pegmatite dike that cross-cuts shear zone fabric near Balliet Lake. Sample 01M127B was collected here. The ~3 cm wide dike is oriented nearly parallel to the outcrop face and nearly perpendicular to the shear zone fabric (NE to right). Note that the thin ''concordant'' felsic metavolcanic layer visible in lower left of photo (*arrow*) is NOT a dike. **c** Outcrop photo of post-kinematic Grt-Ms pegmatite dike that cross-cuts shear zone fabric east of Bompas Lake. The outcrop face is oriented 030/51E and the shear zone fabric is oriented 208/50W

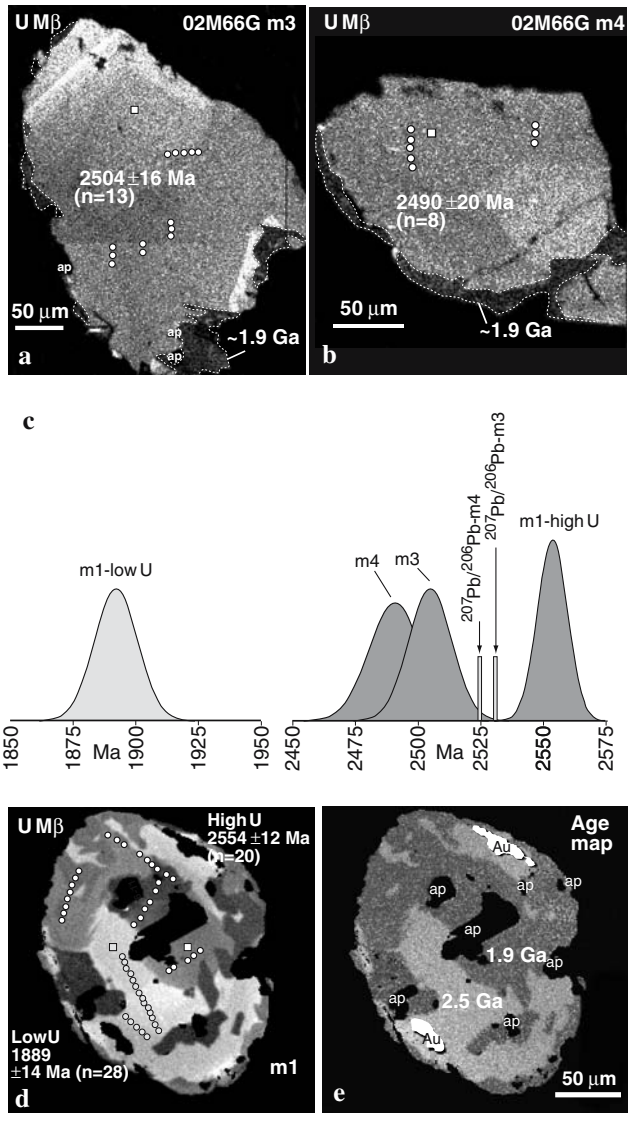

Fig. 6 **a** U M_β X-ray map of 02M66G m3. **b** U M_β X-ray map for m4. **c** Normal distribution curves (e.g., *y*-axis is relative probability) represent EMP dates for m1, m3, and m4. $^{207}Pb/^{206}Pb$ dates from ID-TIMS analysis for m3 and m4 are also shown (heights are arbitrary) **d** U M_β X-ray map of 02M66G m1. **e** Age map of 02M66G m1

samples, two dominant textural and compositional populations of monazite are apparent. Monazite domains of population 1 have relatively low Th and U (<2.0 wt% Th and <0.3 wt% U, Fig. 7b) and occur most commonly as distinct cores surrounded by rims of population 2 (Fig. 9a). Population 2 has a 10–60 μm grain size range and contains 2.5–5.0 wt% Th and 0.3–0.5 wt% U. Monazite of population 2 most commonly occurs in the schistose matrix and some grains are elongate and aligned in the matrix fabric (Fig. 9a). However, some population 2 grains occur as inclusions within plagioclase, cordierite, or garnet but all inclusions except the one occurrence in garnet are either in contact with obvious fractures or are in contact with other included phases (e.g., multi-phase inclusions).

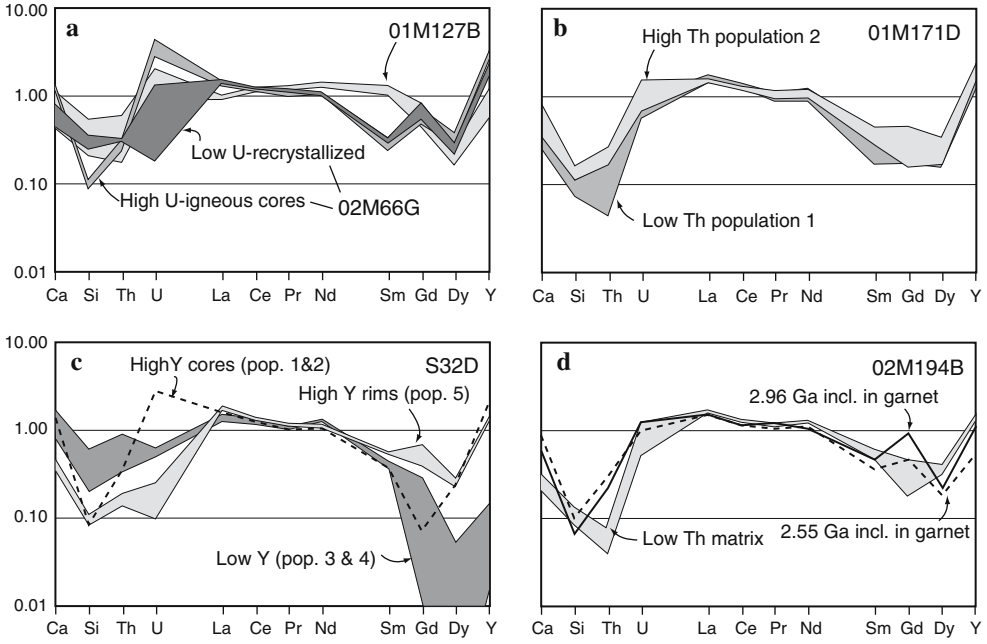

Fig. 7 Major and trace element concentration $\log_{10}$ plots normalized to the composition of an in-house standard, Ward's Elk Mtn monazite

Monazite from population 1 yields dates between 1,872 ± 54 and 1,921 ± 62 Ma in sample 01M171D (Fig. 9) with a weighted mean 1,902 ± 23 Ma (MSWD = 0.44, $n = 5$). Monazite of population 2 yields dates between 1,782 ± 40 and 1,873 ± 42 Ma. Compositional maps show that one matrix grain from sample 01M171D (Fig. 9b) has distinct core and rim domains, both of which are compositionally similar to population 2 but that yield 1,837 ± 40 and 1,794 ± 36 Ma dates, respectively. Although the dates overlap within error, their relative difference and the sharp compositional boundary between the domains suggest that population 2 may represent more than one distinct period of monazite growth. A summary of all monazite data is presented in Fig. 10.

Metamorphic monazite from the East Athabasca mylonite triangle-hanging wall

Mahan et al. (2006) reported EMP monazite data from felsic granulites (peak assemblage Grt-Kfs-Sil-Pl-Qtz) in the Chipman subdomain. Two of these samples are retrograded hydrous granulites (Grt-Crd-Bt-Sil-Pl-Qtz) from the immediate hanging wall of the Legs Lake shear zone (samples S32D and 03M166B) (Fig. 2). The retrograde assemblage is interpreted to have developed during shear zone deformation from the breakdown of earlier high-*P* garnet (Mahan et al. 2003). Mahan et al. (2006) recognized five texturally and compositionally distinct populations of monazite (Fig. 11a) that yielded progressively younger EMP dates ranging from 2.55 to 1.85 Ga (Fig. 10). The fifth and most distinct population occurs as high Y overgrowths that are linked to the synkinematic retrograde hydration reaction Grt + Kfs + H_2O = Bt + Sil + Qtz. This population yielded a weighted mean date of 1,853 ± 15 Ma ($n = 4$) in S32D and 1,851 ± 9 Ma ($n = 3$) in 03M166B (Mahan et al. 2006).

In this study, sample 02M194B was collected from a screen of Grt-Bt-Ms-schist hosted by the ca. 3.0 Ga Chipman tonalite (Hanmer 1997) and surrounded by Grt-Cpx-bearing Chipman mafic dikes near the western margin of the Legs Lake shear zone (Fig. 2). Garnet porphyroblasts are interpreted to have grown during high-grade metamorphism but are extensively resorbed. Retrograde biotite and muscovite define a well-developed retrograde fabric indicating reverse shear sense (Fig. 11b) consistent with kinematics observed throughout the Legs Lake shear zone (Mahan et al 2003). Several populations of monazite were distinguished based on textural setting and composition that yield a range of correlative microprobe dates. Most grains are not significantly zoned, contain 2.0–5.0 wt% Th, and occur both as inclusions in garnet and in the matrix. In addition, several matrix grains have distinctly low Th concentrations (< 1.0 wt%, Fig. 7d). The oldest dates are from monazite grains that are included in garnet (2,975 ± 42 and 2,967 ± 48 Ma). The youngest date from an inclusion in garnet is 2,556 ± 46 Ma and, along with a similar date from a matrix grain, is interpreted to place an upper limit on garnet growth. The low Th matrix grains and the rim of an older grain yielded indistinguishable dates between 1,918 ± 46 and 1,945 ± 76 Ma (weighted mean

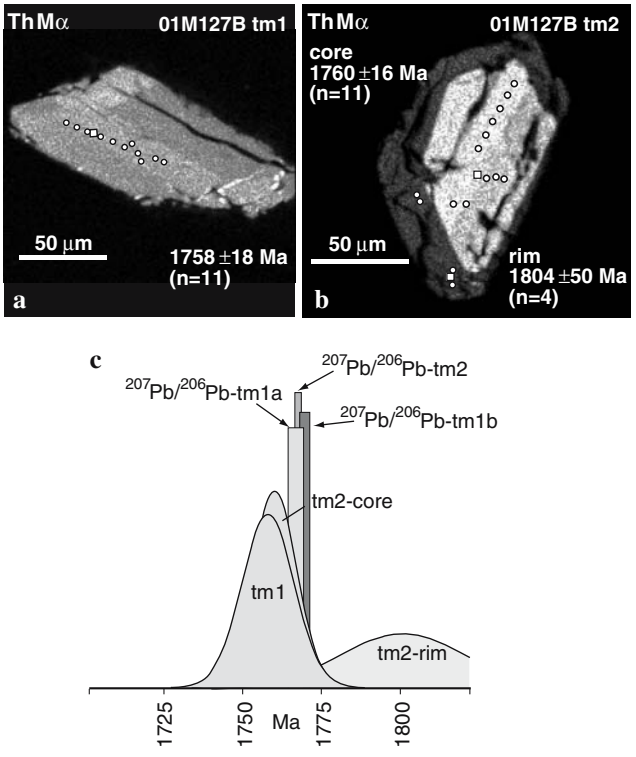

Fig. 8 **a** Th M_α X-ray map of 01M127B tm1. **b** Th M_α X-ray map of 01M127B tm2. **c** Normal distribution curves for EMP dates for tm1 and tm2 (*y*-axis is relative probability). $^{207}Pb/^{206}Pb$ dates from ID-TIMS analysis for tm1 and tm2 are also shown (heights are arbitrary)

1,929 ± 32 Ma; MSWD = 0.23). The matrix grain with the highest Th content in the sample (~5.0 wt% Th) yielded a date of 1,795 ± 24 Ma.

U–Pb ID-TIMS analysis

Analytical methods

Standard crushing and mineral separation techniques produced zircon crystals, which were then air-abraded with pyrite after the method of Krogh (1982), and rinsed and cleaned in an ultrasonic bath of 3M HNO_3. Zircon and monazite fractions were washed and cleaned again in 3M HNO_3 (zircon) or high-purity water (monazite) in savillex beakers, rinsed in distilled acetone and high-purity water, and loaded into Teflon FEP microcapsules. Fractions were spiked with a mixed ^{205}Pb–^{233}U–^{235}U tracer, dissolved in 29 M HF at 220°C for 48–96 h (zircon) or in 12 M HCl at 180°C for 48 h (monazite), followed by conversion to 6 M HCl at 180°C for 12–24 h. Pb and U were chemically separated using anion exchange chemistry, loaded on single Re filaments with a dilute silica gel –0.1 M H_3PO_4 emitter solution, and run on the Massachusetts Institute of Technology VG Sector 54 mass spectrometer. Pb isotopic ratios were measured either by peak-jumping into the axial counting Daly detector, or dynamically with Faraday cups and the Daly detector. U was run as an oxide in static mode. U–Pb data and details regarding isotopic ratio corrections are provided in Table 2. Decay constant uncertainties and U–Pb tracer calibration uncertainties are systematic errors not included in the cited dates.

Analytical results

Deformed granite dikes

A sample of an approximately 1 m wide aplite dike (01M144) was collected near the southeastern arm of Legs Lake where it intrudes a K-feldspar-rich megacrystic Hbl-Bt granite phase of the Stevenson granite (Hanmer 1994, 1997). The aplite is penetratively mylonitized and its crystallization age provides an upper constraint on the age of that deformation as well as a minimum crystallization age for this phase of the Stevenson granite. Six cloudy, ovate, single zircon grains (100 μm long) were analyzed and range from 0.4

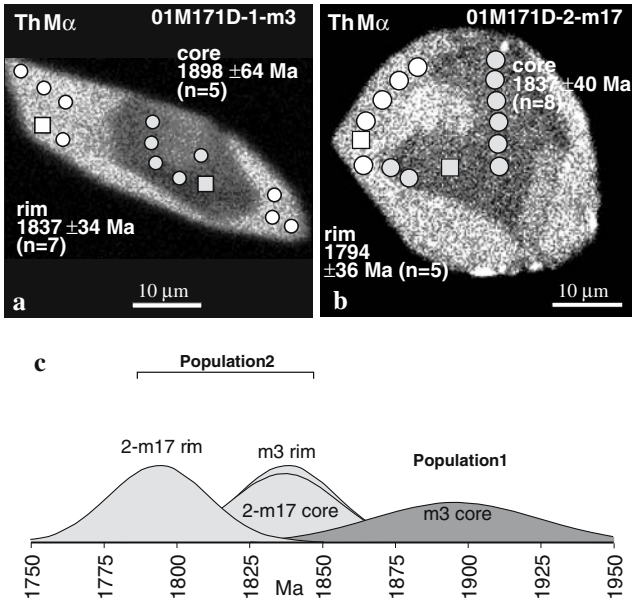

Fig. 9 Th M_α X-ray maps for matrix monazite in biotite schist sample 01M171D. **a** Grain 1-m3. Low Th core (1.4 wt% Th) is population 1. Higher Th rim (2.7 wt%) is population 2. **b** Grain 2-m17. Both relatively low Th core (2.1 wt%) and higher Th rim (2.8 wt%) fall within the compositional range of population 2 based on both Th and U content. However, the contrast in composition and correspondingly different dates for core and rim indicate that population 2 may not represent a single homogeneous age group. **c** Normal distribution curves for EMP dates from 1-m3 and 2-m17 (*y*-axis is relative probability)

to 3.5% normally discordant (Fig. 12a). The two most discordant fractions are excluded from the regression due to the possibility of low temperature Pb loss effects in these high U radiation damaged zircon grains. A York regression through the four most concordant fractions yields an upper intercept of 2616.4 ± 3.6 Ma (MSWD = 0.63), which is interpreted as the crystallization age for this rock.

Two monazite grains from sample 02M66G, with homogenous cores and compositionally distinct rims (m3 and m4) that were previously imaged and analyzed by EMP, were subsequently analyzed by ID-TIMS (Fig. 12b). These grains were extracted from the grain mount, broken into fragments, and lightly air abraded to remove rims prior to TIMS analysis. The $^{207}Pb/^{206}Pb$ dates for m3 and m4 are 2530.7 ± 0.7 and 2524.6 ± 0.7 Ma, respectively. Zircon in sample 02M66G typically consists of clear to cloudy, euhedral prisms 100–300 μm long with aspect ratios from 3:1 to 5:1. Four of the clearest and most euhedral grains were analyzed and range from 0.7 to 2.7% normally discordant (Fig. 12b). The three least concordant fractions do not lie on a common discordia line suggesting either inheritance of zircon of different ages, Pb-loss with a degree of inheritance, or possibly multiple Pb-loss events. The most concordant fraction (z2) has a $^{207}Pb/^{206}Pb$ date of 2530.0 ± 0.7 Ma, consistent with the monazite data. The two monazite analyses and most concordant zircon date suggest a ca. 2,530 Ma crystallization age.

Undeformed Grt-Ms-granite dikes

Four clear, yellow, subhedral to euhedral monazite grains from sample 01M127B, from within the shear zone, were analyzed. Of these, two grains were previously mounted, imaged, and analyzed by EMP (tm1 and tm2). Two concordant and two slightly negatively discordant analyses yielded $^{207}Pb/^{206}Pb$ dates ranging from 1766.2 to 1769.8 Ma. The four analyses yielded a weighted mean of $^{207}Pb/^{206}Pb$ dates of 1767.6 ± 2.4 Ma (MSWD = 6.6), with exclusion of one analysis (tm1b)

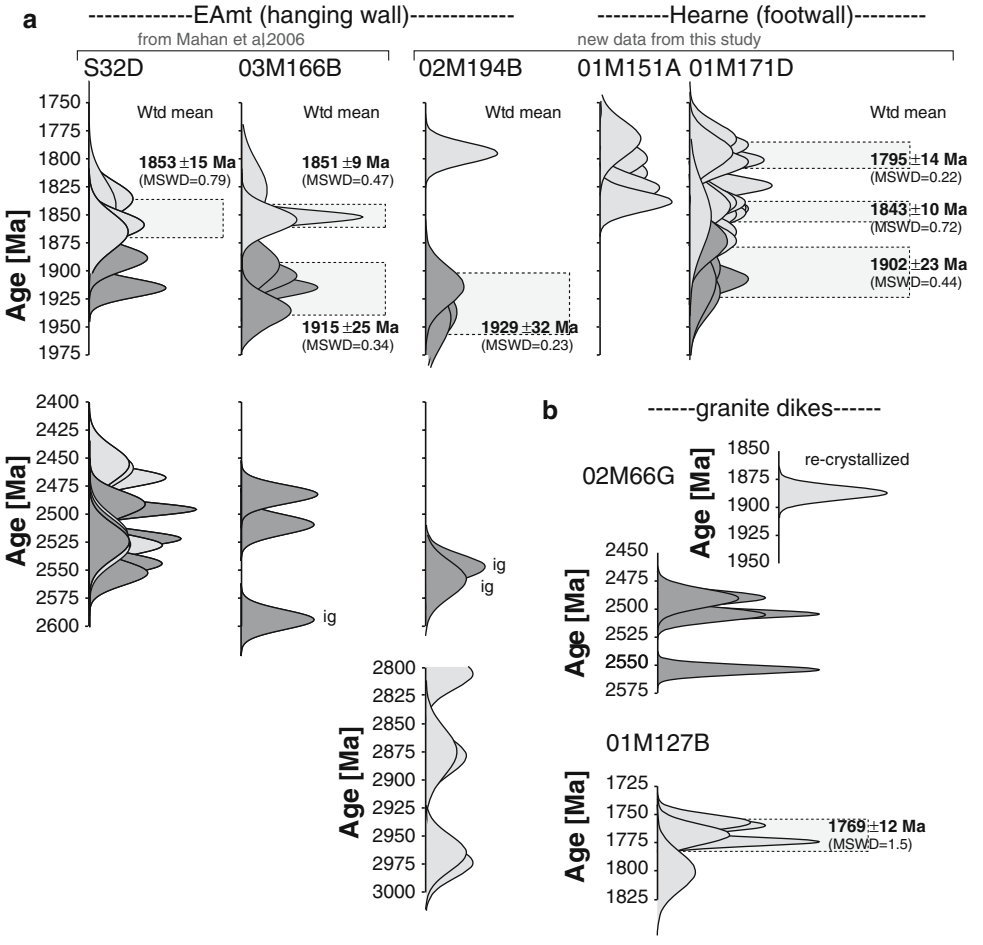

Fig. 10 **a** Summary of electron microprobe monazite ages from the Legs Lake shear zone. Each normal distribution curve represents a single age domain. Note that distribution curves for this figure represent short term random error only (Williams et al. 2006) in order to be comparable to data shown for S32D and 03M166B from Mahan et al. (2006). Shades of gray are used to distinguish age groups. **b** Summary of EMP data from samples 02M66G and 01M127B

yielding a weighted mean $^{207}Pb/^{206}Pb$ date of 1767.0 ± 1.6 Ma (MSWD = 2.3).

Metasediments from the Hearne domain

Analysis of the same monazite grains from sample 01M171D by both EMP and ID-TIMS was not done because of difficulties in handling small grain sizes (30–50 μm mean diameter polished to half size). Five single-grain fractions of monazite from the separate were analyzed by ID-TIMS (Fig. 12d) and are slightly discordant with $^{207}Pb/^{206}Pb$ dates that range from 1,788 to 1,821 Ma. The significance of the spread in dates is discussed in the next section.

Discussion

Comparison of methods and summary of monazite analytical results

Igneous monazite from deformed and undeformed granite dikes

Microprobe dates from monazite in the deformed muscovite granite dike (02M66G) range from 2,490 to 2,554 Ma, with a poorly fit weighted mean of 2,514 ± 34 Ma, and thus are in general agreement with the ca. 2,530 Ma crystallization age suggested from monazite and zircon TIMS data. Two grains with EMP dates of 2,504 ± 16 Ma (m3) and 2,490 ± 20 Ma (m4), were also analyzed directly by ID-TIMS and yielded $^{207}Pb/^{206}Pb$ dates of 2530.8 ± 0.7 and 2524.7 ± 0.7 Ma, respectively (Fig. 6c). The grain-to-grain comparison is in broad agreement although not strictly within their stated error estimates. Differences among the EMP dates and between the EMP and TIMS dates for individual grains are attributed to additional sources of uncertainty in the EMP dates that may contribute to short term systematic error such as calibration and conductive coating thickness or to an underestimate of the background regression uncertainty (Williams et al. 2006).

Microprobe dates from tm1 and tm2 core and rim, from sample 01M127B, are 1,758 ± 18, 1,760 ± 16, and 1,804 ± 50 Ma, respectively (bulk date for tm2 is 1,764 ± 16 Ma). These EMP data agree well with the ID-TIMS $^{207}Pb/^{206}Pb$ dates for these grains (tm1b–1769.8 ± 1.5 Ma, tm2–1767.6 ± 1.0 Ma) (Fig. 8c). The weighted mean EMP date from all five domains is 1,769 ± 12 Ma compared to the ID-TIMS weighted mean $^{207}Pb/^{206}Pb$ date of 1767.6 ± 2.4 Ma.

Metamorphic monazite from metasediments in the Hearne domain

Monazite of population 1 in the Bt-schist in the eastern part of the Legs Lake shear zone (01M171D) yielded a weighted mean date of 1,902 ± 23 Ma that may represent an upper-crustal (Hearne domain) expression of tectonometamorphic events that are better documented in the high-*P* rocks of the hanging wall. At least one phase of deformation and fabric development that pre-dates the Legs Lake shear zone is preserved in Hearne domain rocks in the region (Mahan et al. 2003) and this deformation may correlate with the early monazite population as well. One future test of this will be to evaluate the extent of 1.9 Ga monazite in the Hearne domain ''outside'' of the shear zone where earlier fabrics are better preserved. Berman et al. (2002) also reported a SHRIMP U–Pb date of 1,930 ± 50 Ma for metamorphic monazite in the northwestern Hearne subdomain near Angikuni Lake (Fig. 1a) but relationships between that area and this study area remain to be determined.

Monazite of population 2 is the most dominant and yielded microprobe dates between 1,782 ± 40 and 1,873 ± 42 Ma. At least one grain displays a distinct core and rim, both considered population 2, with EMP dates of 1,837 ± 40 and 1,794 ± 36 Ma (2-m17, Fig. 9b), respectively, and indicates that episodic growth is a likely contributor to the spread in both the EMP and TIMS dates from population 2. Episodic growth is further supported by a pronounced bimodality of EMP dates from all 16 analyzed domains within population 2; peaks occur at ~1,848 Ma and

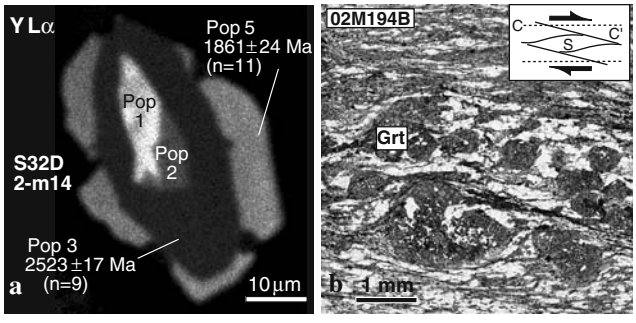

Fig. 11 **a** Y L_α X-ray map of S32D 2-m14 showing four of the five populations distinguished by Mahan et al. (2006). The populations consist of high Y innermost cores (populations 1 and 2), distinctly lower Y domains [populations 3 and 4 (only 3 shown here)], and distinct high Y overgrowths (population 5) that are spatially restricted to the biotite-rich margins of resorbed garnet. Image and dates after Mahan et al. (2006). **b** Photomicrograph of sample 02M194B with record of retrograde S-C-C' mylonitic fabric indicative of reverse sense displacement in Legs Lake shear zone

Table 2 U–Pb isotopic data for monazite and zircon

Fr[a]	Wt (μg)[b]	Composition				Isotopic ratios									Dates (Ma)				Corr. coef.	% Disc.
		U (ppm)	Pb (ppm)	Th[c]/U	Pb[*d]/ Pbc	Pbc[d] (pg)	$^{206}Pb^{e}/^{204}Pb$	$^{208}Pb^{f}/^{206}Pb$	$^{206}Pb^{f}/^{238}U$	% Err[g]	$^{207}Pb^{f}/^{235}U$	% Err[g]	$^{207}Pb^{f}/^{206}Pb$	% Err[g]	$^{206}Pb^{h}/^{238}U$	$^{207}Pb^{h}/^{235}U$	$^{207}Pb^{h}/^{206}Pb$	±		
01M144																				
z2	0.5	370.3	216.1	0.677	47.6	2.4	2554.4	0.190	0.494889	(0.33)	11.9782	(0.34)	0.17554	(0.07)	2591.8	2602.7	2611.2	1.1	0.981	0.9
z3	0.6	260.8	154.8	0.881	61.3	1.5	3223.5	0.254	0.482153	(0.28)	11.6783	(0.33)	0.17567	(0.18)	2536.6	2579.0	2612.4	3.0	0.840	3.5
z4	0.5	295.6	166.1	0.573	66.3	1.2	3730.5	0.162	0.488870	(0.11)	11.7306	(0.12)	0.17403	(0.06)	2565.8	2583.1	2596.8	1.0	0.862	1.5
z5	0.8	476.4	284.3	0.832	130.2	1.7	6921.2	0.235	0.491685	(0.07)	11.8730	(0.09)	0.17513	(0.05)	2578.0	2594.4	2607.3	1.3	0.836	1.4
z7	0.8	113.5	78.1	1.324	12.5	4.8	563.3	0.372	0.493610	(0.42)	11.9163	(0.54)	0.17509	(0.30)	2586.3	2597.8	2606.9	5.0	0.825	1.0
z8	0.8	151.2	98.7	0.887	10.2	7.3	488.1	0.248	0.497268	(0.34)	12.0470	(0.34)	0.17571	(0.07)	2602.0	2608.1	2612.7	1.1	0.980	0.5
02M66G																				
am3	2.0	8127.9	5759.2	1.933	4523.6	2.5	190997.4	0.539	0.481561	(0.06)	11.1079	(0.07)	0.16729	(0.04)	2534.1	2532.2	2530.7	0.7	0.841	–0.2
am4	0.5	20729.6	15000.7	2.093	2101.2	3.6	83345.8	0.586	0.478777	(0.13)	11.0033	(0.14)	0.16668	(0.04)	2521.9	2523.4	2524.6	0.7	0.955	0.1
z1	8.3	1792.9	825.2	0.002	395.0	17.3	22141.3	0.001	0.459189	(0.05)	10.2962	(0.06)	0.16262	(0.04)	2436.0	2461.8	2483.1	0.7	0.771	2.3
z2	6.6	798.0	383.1	0.002	408.2	6.2	23509.0	0.001	0.477366	(0.07)	11.0060	(0.08)	0.16722	(0.04)	2515.8	2523.6	2530.0	0.7	0.834	0.7
z3	6.4	1256.3	589.1	0.005	62.7	59.3	3475.9	0.002	0.460843	(0.14)	10.4300	(0.15)	0.16415	(0.05)	2443.3	2473.7	2498.8	0.9	0.934	2.7
z4	4.0	627.4	297.0	0.006	48.8	23.9	2732.4	0.002	0.464261	(0.09)	10.3983	(0.11)	0.16244	(0.05)	2458.3	2470.9	2481.2	0.9	0.867	1.1
01M127B																				
m2	14.0	3494.2	4618.3	12.78	2843.6	22.7	39795.7	3.720	0.316172	(0.07)	4.7113	(0.08)	0.10807	(0.04)	1771.0	1769.3	1767.2	0.7	0.867	–0.2
m4	2.9	2633.2	3723.0	13.95	1728.2	6.2	23094.2	4.070	0.315292	(0.05)	4.6958	(0.07)	0.10802	(0.04)	1766.7	1766.5	1766.2	0.7	0.794	0.0
tm1b	0.4	1388.1	1754.3	12.04	889.6	0.8	14342.4	3.507	0.316344	(0.09)	4.7206	(0.12)	0.10823	(0.08)	1771.8	1770.9	1769.8	1.5	0.729	–0.1
tm2	0.3	1380.7	1034.8	5.62	271.3	1.1	7368.1	1.640	0.315530	(0.06)	4.7026	(0.09)	0.10809	(0.06)	1767.9	1767.7	1767.5	1.0	0.758	0.0
01M171D																				
m1	0.8	2865.4	2425.5	6.609	359.5	5.4	8238.6	1.933	0.321177	(0.07)	4.8787	(0.08)	0.11017	(0.04)	1795.5	1798.6	1802.2	0.8	0.834	0.4
m3	0.7	1723.7	1577.7	7.38	240.6	4.6	5178.5	2.156	0.323306	(0.08)	4.9337	(0.09)	0.11068	(0.05)	1805.9	1808.0	1810.5	0.9	0.835	0.3
m4	1.4	2554.2	2815.7	9.60	901.6	4.4	16179.5	2.803	0.325274	(0.05)	4.9930	(0.06)	0.11133	(0.04)	1815.4	1818.1	1821.2	0.7	0.761	0.4
m5	0.7	1523.1	1131.6	5.36	81.1	9.7	2089.5	1.570	0.317725	(0.07)	4.7894	(0.09)	0.10933	(0.06)	1778.6	1783.0	1788.2	1.1	0.751	0.6
m6	0.6	1323.5	1022.2	5.56	34.7	17.3	872.6	1.636	0.317436	(0.18)	4.7962	(0.28)	0.10958	(0.21)	1777.2	1784.2	1792.5	3.9	0.651	1.0

[a]All fractions are single grains or fragments. m, monazite; tm, imaged monazite with EMP data; am, imaged monazite with EMP data, abraded prior to TIMS analysis; z, zircon, abraded. Fragments are indicated by a letter after the grain number

[b]Sample weights were estimated to within 40% using measured grain dimensions and a nominal density of 4.5 g/cm^3 for zircon and 5.0 g/cm^3 for monazite

[c]Th contents calculated from radiogenic ^{208}Pb and the $^{207}Pb/^{206}Pb$ date of the sample, assuming concordance between U–Th–Pb systems

[d]Pb* and Pbc represent radiogenic Pb and common Pb, respectively

[e]Measured ratio corrected for fractionation and spike contribution; Pb fractionation was 0.12 ± 0.04%/a.m.u. for Faraday detector or 0.2 ± 0.04%/a.m.u. for Daly detector analysis, based on daily analysis of NBS-981

[f]Measured ratios corrected for fractionation, spike, blank, and initial common Pb; nominal U blank = 0.1 pg ± 50% (2σ); nominal Pb blank = 2.0 pg ± 50% (2σ) for zircon and monazite; initial Pb composition estimated using the model for terrestrial Pb evolution of Stacey and Kramers (1975) at the nominal age of the fraction (i.e., 2.6 or 1.8 Ga)

[g]Numbers in parentheses are the % errors reported at the 2σ confidence interval, propagated using the algorithms of Ludwig (1980)

[h]Isotopic ages calculated using the decay constants of Jaffey et al. (1971): $\lambda(^{235}U) = 9.8485 \times 10^{-10}$ year^{-1} and $\lambda(^{238}U) = 1.55125 \times 10^{-10}$ year^{-1}; error in $^{207}Pb/^{206}Pb$ date reported at the 2σ confidence interval

~1,797 Ma in a cumulative probability diagram (Fig. 13). Using this distribution and a gap in the dates between 1,803 and 1,824 Ma to divide the data into two subsets, the weighted mean of 11 older domains is 1,843 ± 10 Ma (MSWD = 0.72) and of the remaining five younger domains is 1,795 ± 14 Ma (MSWD = 0.22).

Five monazite grains from the Bt-schist have near concordant ID-TIMS $^{207}Pb/^{206}Pb$ dates ranging from 1,788 to 1,821 Ma, which are encompassed by the range of EMP dates from population 2. A concordant to near concordant spread in isotopic dates over ten's of millions of years is a relatively common characteristic for metamorphic monazite (e.g., Hawkins and Bowring 1997, 1999; Harrison et al. 2002; Gibson et al. 2004). Possible explanations for this behavior include physical mixtures of monazite of different but relatively closely spaced ages (i.e., inheritance; Parrish 1990; Gibson et al. 2004), protracted growth during metamorphism or hydrothermal fluid flow (Hawkins and Bowring 1997, 1999; Harlov and Förster 2003), and high temperature Pb loss (Parrish 1990). The latter seems most unlikely given recent studies suggesting that the closure temperature for Pb in monazite by volume diffusion approaches 900–1,000°C (e.g., Crowley and Ghent 1999; Cherniak et al. 2004). Given the evidence from X-ray maps and EMP dates for population 2 consisting of multiple growth episodes between ~1,850 and 1,790 Ma and the lack of evidence for monazite younger than ~1,790 Ma, we suggest that physical mixing of monazite with a similar multiple growth history is the most significant contributor to the spread in the TIMS dates from 01M171D. However, it is noted that a simple mixing line between ~1,850 and ~1,790 Ma would lie slightly left of some analyses. Therefore small amounts of inheritance from older monazite (although population 1 is not clearly represented in the data), effects from inaccuracies in the U decay constants (Mattinson 1994; Schoene et al. 2006), or Pb loss via unknown mechanisms other than volume diffusion may not be ruled out.

In summary, we consider the two datasets to agree quite well and the results from each approach lend useful insight into the interpretation of the other. TIMS analysis provides the time-tested reliability for dating zircon and monazite with high precision that is needed for determining the crystallization ages of the important rock units in the shear zone as well as for cross-checking the EMP results. X-ray mapping, ''age''-mapping, and microprobe trace element analysis of monazite all help to reveal grain-scale complexities (e.g., recrystallized zones), distinct textural/compositional populations that can be linked to specific metamorphic and/or deformation processes (e.g., high Y monazite overgrowths in retrograde felsic granulites), and multiple monazite age populations that might otherwise make a conventional isotopic dataset difficult to uniquely interpret.

Metamorphic monazite from the East Athabasca mylonite triangle-hanging wall

The monazite dataset from the sample of retrogressed felsic granulite (02M194B) has some clear distinctions from, as well as similarities to, the datasets from the felsic granulites of Mahan et al. (2006) and Baldwin et al. (2006). Prior to this study, the oldest monazite recognized in the East Athabasca region was ca. 2.6–2.5 Ga. Middle Archean monazite (ca. 2.96 Ga) from this sample clearly indicates a distinctly different and older protolith than other monazite-bearing granulites in the region and may reflect an early phase of regional metamorphism or perhaps more local effects associated with late-stage emplacement of the host tonalite complex. Crocker et al. (1993) also interpreted U–Pb, Sm–Nd, and Rb–Sr data to reflect a ca. 2.9 Ga metamorphic event in middle Archean gneisses from the Rae domain south of the Athabasca basin. The two major episodes of high-*P* granulite-facies metamorphism, at 2.55 and 1.9 Ga, are represented by monazite age groups in this sample as well as in the three Chipman subdomain felsic granulites from Mahan et al. (2006). In all samples, the late Archean monazite grains are the youngest inclusions in garnet, which is consistent with the interpretation that the garnet-bearing metamorphic assemblage initially developed during late Archean metamorphism (Baldwin et al. 2006; Mahan et al. 2006). Thus, monazite was an effective recorder of events over a long (>1,000 million year) and complex history of tectonometamorphism in the high-*P* terrane. However, only post-1.9 Ga monazite populations, which appear to be relatively minor by volume and to have only developed in certain rock types, are related to the regional exhumation history. For example, despite the extensive synkinematic retrogression and garnet resorption, sample 02M194B does not contain the well-developed high Y overgrowths recognized in the other two retrograded felsic granulites (S32D and 03M166B), presumably reflecting differences in the bulk phosphorus and/or LREE budgets and different major silicate retrograde reactions. Where present, post-1.9 Ga monazite appears to have only developed in distinct shear zones (e.g., Legs Lake shear zone) where concentrated fluid flow and extensive retrograde metamorphic reactions provided the conditions and facilitated the production of chemical constituents necessary for new monazite growth

(Mahan et al. 2006). In contrast, the rocks further removed from zones of active deformation during exhumation preserve their peak assemblages and did not develop post-1.9 Ga monazite.

Timing of Legs Lake shear zone movement and metamorphism in the Hearne domain

General constraints

Several lines of evidence provide general constraints for the timing of deformation in the Legs Lake shear zone to between 1.9 and 1.79 Ga. Although we report new crystallizations ages of 2614.5 ± 2.5 Ma and ca. 2,530 Ma for deformed intrusions within the shear zone, the 1896.7 ± 0.8 Ma age for high pressure partial melting and inferred emplacement of Chipman mafic dikes (Flowers et al. 2006a), which were subsequently deformed at amphibolite-facies in the shear zone, provides a Proterozoic upper bound. A lower bound is provided by our new crystallization age of 1767.6 ± 2.4 Ma for an undeformed Grt-Ms-granite dike that cross-cuts the shear zone fabric. In addition, the northern end of the Legs Lake shear zone, where it bounds the East Athabasca mylonite triangle, is offset dextrally by 110 km to the northeast across the Grease River shear zone (Mahan and Williams 2005). A ca. 1,800 Ma age of this younger structure is suggested by a preliminary zircon date of 1,788+28/–15 Ma that was reported by Hanmer (1997) from a syn-kinematic granitic dike and by preliminary 1,810–1,800 Ma syn-kinematic monazite dated by electron microprobe (Williams and Jercinovic 2002).

Metamorphic monazite growth

With respect to the Legs Lake shear zone, microstructural observations indicate synkinematic prograde metamorphism in metapelites from the Hearne domain footwall whereas peak metamorphism of those rocks was reached late to post-kinematically (Mahan et al. 2003). The dominant population (#2) of monazite in these rocks involves two main periods of monazite growth, an earlier one approximated at 1,843 ± 10 Ma and a younger one at 1,795 ± 14 Ma. The older period is indistinguishable from 1,853 ± 15 Ma monazite from the hanging wall of the shear zone, which Mahan et al. (2006) linked to synkinematic retrograde reactions in felsic granulites. Similarly, we interpret the older period of monazite growth in the Hearne domain rocks to correspond to shear zone deformation and early prograde metamorphism in the footwall. The younger monazite growth may correspond to peak metamorphism in the footwall or may be related to a renewed period of heating and/or fluid circulation associated with regional Hudsonian magmatism (Peterson et al. 2002). We suggest the former, which is supported by recognition of monazite growth and peak metamorphism at ca. 1,810 Ma in other localities beneath and south of the Athabasca basin in the western Hearne domain (Orrell et al. 1999; Anneseley et al. 2005).

Implications for regional exhumation of deep-crustal rocks in the East Lake Athabasca region

It is important to distinguish between relatively early periods of local or differential exhumation of individual domains and subdomains and what may represent ''regional'' exhumation of the high-*P* terrane as a whole. Several studies suggest that much of the East Athabasca region first experienced high-*P* (~1.0+ GPa) metamorphic conditions at ca. 2.6–2.5 Ga (e.g., Hanmer 1997; Flowers 2005; Williams and Hanmer 2005), but the spatial extent of this early high-*P* event is not yet known. For example, although relatively little work has been done, there appears to be no evidence for late Archean high-*P* metamorphism in much of the adjacent Rae domain, west of the Grease River shear zone. However, abundant evidence points to high-*P* granulite conditions in those rocks at 1.9 Ga. Thus, both differential loading and exhumation of specific domains and/or subdomains during the 600 million year interval of 2.5–1.9 Ga is possible. Some evidence for differential exhumation within the East Athabasca mylonite triangle is provided by Baldwin et al. (2003, 2004), who suggested that rocks in the southern subdomain were decompressed from >1.5 to 1.0 GPa between 1,904 and 1,895 Ma. However, by ca. 1.9 Ga, the entire region, consisting of an area >20,000 km^2, was apparently resident in the deep crust at relatively uniform pressures of 0.9–1.1 GPa. Subsequent ''regional'' exhumation of this area occurred over the next ~150 million years during several distinct episodes (see also Flowers et al. 2006b).

Regional exhumation: phase 1

Petrologic observations from several localities within the East Athabasca region (Neil Bay, Kopf 1999; southern subdomain, Kopf 1999; Wholdaia Lake, Krikorian 2002; Chipman subdomain—K.H. Mahan, unpublished data) indicate a decompression phase shortly following peak metamorphism. Late textures and retrograde assemblages in mafic granulites record

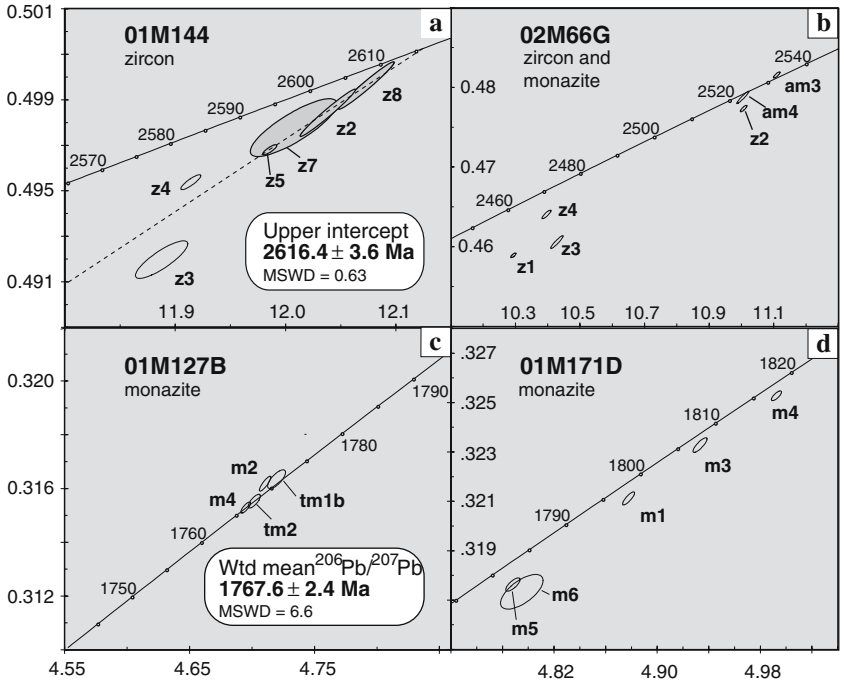

Fig. 12 U–Pb concordia diagrams. **a** 01M144. *Shaded ellipses* are analyses used for regression line. **b** 02M66G. **c** 01M127B. **d** 01M171D

localized re-equilibrated conditions of 0.8–0.7 GPa and 700–750°C suggesting that a phase of relatively high temperature decompression immediately followed 1.9 Ga metamorphism. This is also consistent with an early stage of anhydrous decompression interpreted from petrologic modeling of retrograde felsic granulites from the Legs Lake shear zone hanging wall (Mahan et al. 2006). Further north in the western Churchill Province, Sanborn-Barrie et al. (2001) suggested rapid ~1.9 Ga decompression of the high-*P* Kramanituar complex (Fig. 1) via buoyancy-driven extensional unroofing and a similar mechanism may have been involved here, as suggested by Flowers et al. (2006a) who inferred an extensional regime during emplacement and metamorphism of the Chipman mafic dike complex.

Regional exhumation: phase 2

The second phase of regional exhumation occurred approximately 40–50 million year after 1.9 Ga thermotectonic events in the East Athabasca region, which may imply a period of (isobaric?) cooling towards a steady-state geotherm during that interval (Fig. 14). Based on data from this study, we suggest that renewed rock uplift involved ca. 1,850 Ma east-vergent thrusting of the high-*P* terrane across the Legs Lake shear zone. Rocks in the immediate hanging wall of the shear zone record retrograde conditions of 0.4–0.5 GPa and ~550–600°C (Mahan et al. 2003, 2006). Hearne rocks in the footwall record a syn-kinematic prograde metamorphic path from andalusite stability (< 0.4 GPa) to peak conditions of 0.5 GPa (maximum) and ~600°C (Fig. 14; Mahan et al. 2003). Thus, assuming hanging wall rocks were at 0.8 GPa and footwall rocks were at 0.3 GPa prior to shear zone initiation, subsequent thrusting accommodated ~15–20 km (equivalent to 0.5 GPa) of uplift of the hanging wall relative to the downgoing Hearne domain. Synchronous decompression and re-equilibration of rocks in the hanging wall at shallower levels implies that denudation processes such as erosion and/or extensional faulting operated at higher structural levels during the thrusting process (e.g., Jamieson and Beaumont 1989). This re-equilibration further implies another period of near isobaric cooling (Fig. 14) at middle crustal levels prior to the third and final phase of exhumation.

Contractional deformation in the Legs Lake shear zone at ca. 1,850 Ma coincides with and was probably driven by early convergence across the Trans-Hudson orogen to the southeast (Fig. 1). A major continental magmatic arc developed at the southeastern margin of the Hearne domain between 1,865–1,850 Ma (Wathaman–Chipewyan batholith; Bickford et al. 1990; Meyer et al. 1992; Corrigan et al. 2005). Northwest-directed accretion of one or more island arc terranes began at ca. 1,850. Terminal continent–continent collision of the Superior and Hearne cratons had begun by ca. 1,835 (Bickford et al. 1990; Orrell et al. 1999; Corrigan et al. 2005) and produced significant crustal shortening and associated peak and post-collisional

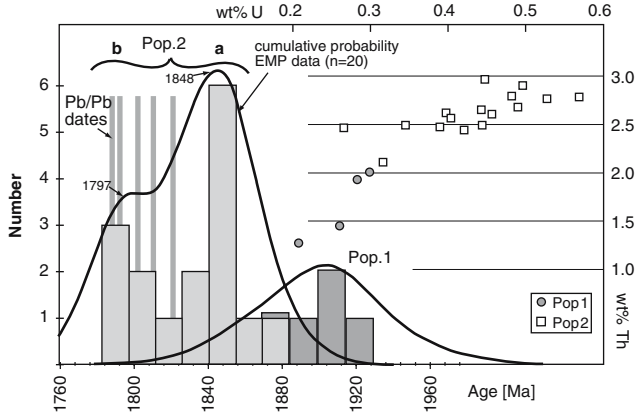

Fig. 13 Cumulative probability plot (*x*-axis is EMP date) and Th versus U composition plot (right and top axis labels) for 20 monazite domains from sample 01M171D. Note the three peaks in the probability curve. The oldest peak at ca. 1.9 Ga corresponds to population 1. The distribution of population 2 monazite consists of two peaks at ~1,848 and 1,797 Ma. Also shown for comparison are the $^{207}Pb/^{206}Pb$ dates for five monazite grains analyzed by TIMS. The histogram and probability curve were created with Isoplot/Ex Version 3 (Ludwig 2003)

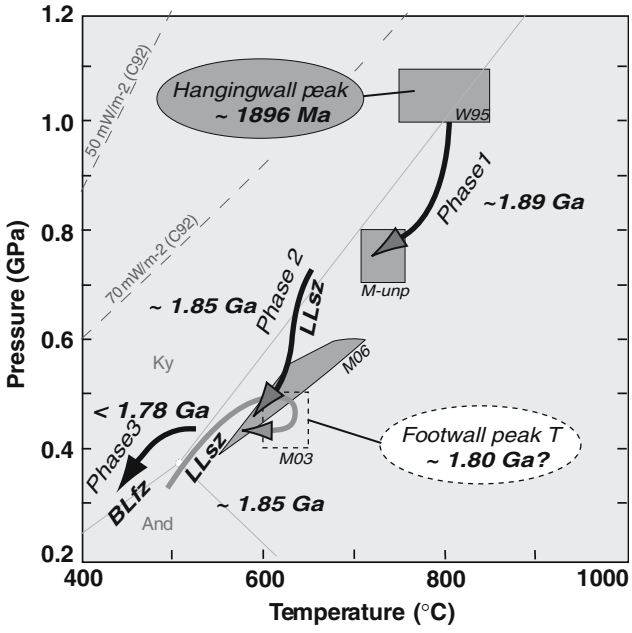

Fig. 14 *P–T* diagram for Chipman subdomain and Hearne domain. *Dark gray P–T* path segments—Chipman subdomain (hanging wall of Legs Lake shear zone [*LLsz*]). *Light gray segment*—Hearne domain (footwall). *Solid black segment*—hanging wall and footwall. *Shaded*and *unshaded rectangles* represent the range of thermobarometric results from Chipman subdomain (peak-W95-Williams et al. 1995; intermediate retrograde-M-unp-Mahan, unpublished data) and footwall peak (M03-Mahan et al. 2003). Irregular shaded region is modeled stability field of retrograde assemblage in hanging wall felsic granulite from Mahan et al. 2006 (M06). Timing of peak metamorphism in hanging wall is from Flowers et al. (2006a). BLfz-Black Lake fault zone. *Thin dashed lines* are steady state geotherms from Chapman and Furlong (1992)

metamorphism in the Hearne domain (e.g., Lewry and Sibbald 1980; Lewry and Collerson 1990; Bickford et al. 1994; Orrell et al. 1999; Ross et al. 2000; Aspler et al. 2002; Annesley et al. 2005).

Regional exhumation: phase 3

The third phase of exhumation involved the removal of 15–20 km of overburden from both hanging wall and footwall and most likely, over a much larger region. Exhumation could have occurred primarily by erosion, but a greenschist-facies ductile to brittle extensional reactivation of part of the Legs Lake shear zone along the NW-dipping Black Lake fault zone suggests a component of tectonic denudation as well (Mahan et al. 2003). This is consistent with other workers' suggestions that extensional faulting helped accommodate regional exhumation of the southern Hearne domain (e.g., Orrell et al. 1999; Annesley et al. 2005). The age of the Black Lake fault zone is constrained to between the end of deformation in the Legs Lake shear zone and initiation of deposition in the ca. 1.7 Ga Athabasca basin. However, the faulting also involved a sinistral strike-slip component and thus may correlate with ca. 1,775–1,760 Ma sinistral faults that developed in the basement beneath the eastern Athabasca basin (Annesley et al. 2005).

Poly-phase exhumation of large deep crustal terranes

Recognition of the poly-phase nature of the exhumation process in the East Lake Athabasca area, involving at least three distinct phases over a ~150 million year period, is particularly important for the development and evaluation of evolutionary models for this region. This is similar to other studies that have concluded that the exposure of deep continental crustal terranes commonly involves more than one distinct period of exhumation. For example, the deepest levels of the Kapuskasing zone record evidence for at least two phases of exhumation prior to ca. 1,900–1,850 Ma thrust-related uplift across the Ivanhoe Lake fault (Percival and West 1994), the structure with which exhumation of this well-known region is most commonly associated. Similarly, multi-phase exhumation of deep crustal granulite terranes is suggested for the Ivrea Zone in the Italian Alps (e.g., Handy and Zingg 1991), western Fiordland, New Zealand (e.g., Klepeis et al. 1999; cf. Flowers et al. 2005), and the Arunta block bounded by the Red Bank thrust in central Australia (e.g., Biermeier et al. 2003). The Legs Lake shear zone, as well as its along strike equivalents, appears to be a higher-grade analogy to other major

bounding thrust faults, such as the Red Bank and Ivanhoe thrust zones whose movement occurred at a distinctly younger time than that of peak granulite-facies events in their hanging walls.

Conclusions

1. The combination of in situ analytical techniques, such as EMP monazite dating, with high-precision ID-TIMS analysis, provides an exceptional geochronological approach to the study of complex polymetamorphic and multiply deformed terrains. In addition, X-ray compositional maps of full thin sections and individual grains, ''age'' maps, and trace element compositions provide essential information for linking monazite to metamorphic and deformation processes and for interpretations of complex geochronological datasets.
2. An undeformed granite dike in the Legs Lake shear zone yields a crystallization age and minimum timing constraint on deformation of 1767.6 ± 2.4 Ma. The youngest deformed rock in the shear zone that has been directly dated yields a ca. 2,530 Ma crystallization age, but the previously reported 1896.7 ± 0.8 Ma age of high-*P* metamorphism in the hanging wall represents a tighter maximum age constraint on deformation. Several monazite age groups are apparent from hanging wall and footwall samples and range from >2,900 to ca. 1,800 Ma. We interpret 1,843 ± 10 Ma monazite to coincide with the timing of shear zone deformation and early prograde metamorphism in the footwall, which correlates well with previously reported 1,853 ± 15 Ma monazite growth associated with major retrograde metamorphism and shear zone deformation in the hanging wall.
3. The exhumation history of rocks in the East Athabasca region prior to 1.9 Ga was not spatially uniform and may have involved several pulses of differential exhumation of individual blocks. The nature and tectonic significance of these events is still not clear, but available data suggest that a region comprising an area of at least 20,000 km^2 was resident at 0.9–1.1 GPa by 1.9 Ga. Subsequent exhumation of the region occurred during at least three phases over the next 150–200 million years. The first phase was characterized by relatively high-temperature decompression during or immediately following 1.9 Ga tectonometamorphism. We interpret the second phase of regional exhumation to have involved east-vergent thrusting in the Legs Lake shear zone at ca. 1,850 Ma, which may have been driven by convergence across the Trans-Hudson orogen. The final phase of exhumation after ~1.78 Ga likely involved extensional faulting and was complete by ca. 1.70 Ga deposition of the overlying Athabasca basin.

Acknowledgements This research was funded in part by National Science Foundation grant EAR 0001152 to MLW and SAB and by a GSA student research grant to KHM. Some field support given by the Geological Survey of Canada is greatly appreciated. We thank Randy Parrish and Calvin Miller for thoughtful and constructive formal reviews, and we appreciate numerous discussions with G. Dumond and P. Goncalves that helped shape the ideas presented here.

References

Annesley IR, Madore C, Portella P (2005) Geology and thermotectonic evolution of the western margin of the THO: evidence from the eastern sub-Athabasca basement, Saskatchewan. Can J Earth Sci 42:573–597

Aspler LB, Chiarenzelli JR, McNicoll VJ (2002) Paleoproterozoic basement-cover infolding and thick-skinned thrusting in Hearne domain, Nunavut, Canada: intracratonic response to Trans-Hudson orogen. Precambrian Res 116:331–354

Baldwin JA, Bowring SA, Williams ML (2003) Petrologic and geochronologic constraints on high-pressure, high-temperature metamorphism in the Snowbird tectonic zone, Canada. J Metamorph Geol 21:81–98

Baldwin JA, Bowring SA, Williams ML, Williams IS (2004) Eclogites of the Snowbird tectonic zone: petrological and U–Pb geochronological evidence for Paleoproterozoic high-pressure metamorphism in the western Canadian Shield. Contrib Mineral Petrol 147:528–548

Baldwin JA, Bowring SA, Williams ML, Mahan KH (2006) Geochronological constraints on the evolution of high-pressure felsic granulites from an integrated electron microprobe and ID-TIMS geochemical study. Lithos 88:173–200

Berman RG, Davis WJ, Aspler LB, Chiarenzelli JR (2002) SHRIMP U–Pb ages of multiple metamorphic events in the Angikuni Lake area, western Churchill province, Nunavut. Current Research (Paper 2002-F3):9 p

Bickford ME, Collerson KD, Lewry JF, Van Schmus WR, Chiarenzelli JR (1990) Proterozoic collisional tectonism in the Trans-Hudson orogen, Saskatchewan. Geology 18:14–18

Bickford ME, Collerson KD, Lewry JF (1994) Crustal history of the Rae and Hearne provinces, southwestern Canadian Shield, Saskatchewan: contraints from geochronologic and isotopic data. Precambrian Res 68:1–21

Biermeier C, Stuwe K, Foster DA, Finger F (2003) Thermal evolution of the Redbank thrust system, central Australia: geochronological and phase-equilibrium constraints. Tectonics 22(1):1–23

Chapman DS, Furlong KP (1992) Thermal state of the continental lower crust. In: Fountain DM, Arculus R, Kay RW (eds) Continental lower crust: developments in geotectonics, vol 23. Elsevier, Amsterdam, pp 179–199

Cherniak DJ, Watson EB, Grove M, Harrison TM (2004) Pb diffusion in monazite: a combined RBS/SIMS study. Geochim Cosmochim Acta 68:829–840

Corrigan D, Hajnal Z, Németh B, Lucas SB (2005) Tectonic framework of a Paleoproterozoic arc–continent to continent–continent collisional zone, Trans-Hudson Orogen, from geological and seismic reflection studies. Can J Earth Sci 42:421–434

Crocker CH, Collerson KD, Lewry JF, Bickford ME (1993) Sm–Nd, U–Pb, and Rb–Sr geochronology and lithostructural relationships in the southwestern Rae province: constraints on crustal assembly in the western Canadian shield. Precambrian Res 61:27–50

Crowley JL, Ghent ED (1999) An electron microprobe study of the U–Th–Pb systematics of metamorphosed monazite: the role of Pb diffusion versus overgrowth and recrystallization. Chem Geol 157:285–302

Cumming GL, Krstic D, Wilson JA (1987) Age of the Athabasca Group, northern Alberta. Geological Association of Canada—Mineralogical Association of Canada, Annual Meeting, Program with abstracts, 12:35

Flowers RM (2005) Stabilization, reactivation, and exhumation of cratonic lithosphere: a view from the lower crust, East Lake Athabasca area, western Canadian shield. PhD dissertation, Massachusetts Institute of Technology, pp 222

Flowers RM, Bowring SA, Tulloch AJ, Klepeis KA (2005) Tempo of burial and exhumation within the deep roots of a magmatic arc, Fiordland, New Zealand. Geology 33:17–20

Flowers RM, Bowring SA, Williams ML (2006a) Timescales of high-pressure, high-temperature metamorphism and mafic dike anatexis, Snowbird tectonic zone, Canada. Contrib Mineral Petrol 151:558–581

Flowers RM, Mahan KH, Bowring SA, Williams ML, Pringle MS, Hodges KV (2006b) Multistage exhumation and juxtaposition of lower continental crust in the western Canadian Shield: linking high-resolution U–Pb and $^{40}Ar/^{39}Ar$ thermochronometry with *P–T–D* paths. Tectonics (in press)

Foster G, Parrish RR, Horstwood MSA, Chenery S, Gibson HD (2004) The generation of prograde *P–T–t* points and paths; a textural, compositional, and chronological study of metamorphic monazite. Earth Planet Sci Lett 228:125–142

Fountain DM, Salisbury MH (1981) Exposed cross sections through the continental crust: implications for crustal structure, petrology and evolution. Earth Planet Sci Lett 5:263–277

Gibson HD, Carr SD, Brown RL, Hamilton MA (2004) Correlations between chemical and age domains in monazite, and metamorhic reactions involving major pelitic phases: an integration of ID-TIMS and SHRIMP geochronology with Y–Th–U X-ray mapping. Chem Geol 211:237–260

Goncalves P, Williams ML, Jercinovic MJ (2005) Electron microprobe age mapping of monazite. Am Mineral 90:578–585

Goodacre AK, Grieve RAF, Halpenny JF, Sharpton VL (1987) Horizontal gradient of the Bouguer gravity anomaly map of Canada, Canadian Geophysical Atlas, Map 5

Green AG, Milkereit B, Davidson A, Spencer C, Hutchinson DR, Cannon WF, Lee MW, Agena WF, Behrendt JC, Hinze WJ (1988) Crustal structure of the Grenville front and adjacent terranes. Geology 16:788–792

Handy MR (1990) The exhumation of cross-sections of the continental crust: structure, kinematics and rheology. In: Salisbury MH, Fountain DM (eds) Exposed cross-sections of the continental crust. Kluwer, Dordrecht, pp 485–507

Handy MR, Zingg A (1991) The tectonic and rheological evolution of an attenuated cross-section of the continental crust—Ivrea crustal section, southern Alps, northwest Italy and southern Switzerland. Geol Soc Am Bull 103:236–253

Hanmer S (1994) Geology, East Athabasca mylonite triangle, Saskatchewan. Geol Surv Can Map 1859A

Hanmer S (1997) Geology of the Striding-Athabasca mylonite zone, northern Saskatchewan and southeastern District of Mackenzie, Northwest Territories. Geol Surv Can Bull, p 92

Hanmer S, Parrish R, Williams ML, Kopf C (1994) Striding-Athabasca mylonite zone: complex Archean deep-crustal deformation in the East Athabasca mylonite triangle, N. Saskatchewan. Can J Earth Sci 31:1287–1300

Hanmer S, Williams ML, Kopf C (1995a) Striding-Athabasca mylonite zone: implications for Archean and Early Proterozoic tectonics of the western Canadian Shield. Can J Earth Sci 32:178–196

Hanmer S, Williams ML, Kopf C (1995b) Modest movements, spectacular fabrics in an intracontinental deep-crustal strike-slip fault: Striding-Athabasca mylonite zone, NW Canadian Shield. J Struct Geol 17:493–507

Harlov DE, Förster HJ (2003) Fluid-induced nucleation of (Y + REE)-phosphate minerals within apatite: nature and experiment. Part II. Flourapatite. Am Mineral 88:1209–1229

Harlov DE, Förster HJ, Nijland TG (2002) Fluid-induced nucleation of REE-phosphate minerals in apatite: nature and experiment. Part I. Chlorapatite. Am Mineral 87:245–261

Harrison TM, Catlos EJ, Montel JM (2002) U–Th–Pb dating of phosphate minerals. Rev Mineral Geochem 48:523–577

Hawkins DP, Bowring SA (1997) U–Pb systematics of monazite and xenotime: case studies from the Paleoproterozoic of the Grand Canyon, Arizona. Contrib Mineral Petrol 127:87–103

Hawkins DP, Bowring SA (1999) U–Pb monazite, xenotime and titanite geochronological constraints on the prograde to post-peak metamorphic thermal history of Paleoproterozoic migmatites from the Grand Canyon, Arizona. Contrib Mineral Petrol 134:150–169

Hoffman PF (1988) United plates of America, the birth of a craton: Early Proterozoic assembly and growth of Laurentia. Annu Rev Earth Planet Sci 16:543–603

Jaffey AH, Flynn KF, Glendenin LE, Bentley WC, Essling AM (1971) Precision measurements of half-lives and specific activities of ^{235}U and ^{238}U. Phys Rev C4:1889–1906

Jamieson RA, Beaumont C (1989) Deformation and metamorphism in convergent orogens: a model for uplift and exhumation of metamorphic terrains. In: Daly JS, Cliff RA, Yardley BWD (eds) Evolution of metamorphic belts, Special Publication 43. Geol Soc London, pp 117–129

Jercinovic MJ, Williams ML (2005) Analytical perils (and progress) in electron microprobe trace element analysis applied to geochronology: background acquisition, interferences, and beam irrradiation effects. Am Mineral 90:526–546

Klepeis KA, Daczko NR, Clarke GL (1999) Kinematic vorticity and tectonic significance of superposed mylonites in a major lower crustal shear zone, northern Fiordland, New Zealand. J Struct Geol 21:1385–1405

Kohn MJ, Malloy MA (2004) Formation of monazite via prograde metamorphic reactions among common silicates: implications for age determinations. Geochim Cosmochim Acta 68:101–113

Kopf C (1999) Deformation, metamorphism, and magmatism in the East Athabasca mylonite triangle, northern Saskatchewan: implications for the Archean and Early Proterozoic crustal structure of the Canadian Shield. PhD dissertation, University of Massachusetts-Amherst, p 139

Kretz R (1983) Symbols for rock-forming minerals. Am Mineral 68:277–279

Krikorian L (2002) Geology of the Wholdaia Lake segment of the Snowbird Tectonic Zone, Northwest Territories (Nunavut): a view of the deep crust during assembly and stabilization of the Laurentian craton. MSc Thesis, University of Massachusetts-Amherst, p 90

Krogh TE (1982) Improved accuracy of U–Pb zircon ages by the creation of more concordant systems using an abrasion technique. Geochim Cosmochim Acta 46:637–649

Lewry JF, Collerson KD (1990) The Trans-Hudson Orogen: extent, subdivisions and problems. In: Lewry JF, Stauffer MR (eds) The Early Proterozoic Trans-Hudson Orogen of North America, Geological Association of Canada Special Paper 37, pp 1–14

Lewry JF, Sibbald TII (1980) Thermotectonic evolution of the Churchill Province in northern Saskatchewan. Tectonophysics 68:5–82

Ludwig KR (1980) Calculation of uncertainties of U–Pb isotope data. Earth Planet Sci Lett 46:212–220

Ludwig KR (2003) Isoplot/Ex Version 3.00: a geochronological toolkit for Microsoft Excel, Berkeley Geochronology Center

Mahan KH, Williams ML (2005) Reconstruction of a large deep crustal exposure: implications for the Snowbird Tectonic Zone and early growth of Laurentia. Geology 33:385–388

Mahan KH, Williams ML, Baldwin JA, Bowring SA (2001) Juxtaposition of deep crustal and middle crustal rocks across the Legs Lake shear zone in northern Saskatchewan, Summary of Investigations 2001, Saskatchewan geological survey

Mahan KH, Williams ML, Baldwin JA (2003) Contractional uplift of deep crustal rocks along the Legs Lake shear zone, western Churchill Province, Canadian Shield. Can J Earth Sci 40:1085–1110

Mahan KH, Goncalves P, Williams ML, Jercinovic MJ (2006) Dating metamorphic reactions and fluid flow: application to exhumation of high-*P* granulites in a crustal-scale shear zone, western Canadian shield. J Metamorph Geol 24:193–217

Mattinson JM (1994) Uranium decay constant uncertainties and their implications for high-resolution U–Pb geochronology. GSA Abst Prog 77:A-221

Meyer MT, Bickford ME, Lewry JF (1992) The Wathamun batholith: an early Proterozoic continental arc in the Trans-Hudson belt, Canada. Geol Soc Am Bull 104:1073–1085

Montel JM, Foret S, Veschambre M, Nicollet C, Provost A (1996) Electron microprobe dating of monazite. Chem Geol 131:37–53

Orrell SE, Bickford ME, Lewry JF (1999) Crustal evolution and age of thermotectonic reworking in the western hinterland of the Trans-Hudson Orogen, northern Saskatchewan. Precambrian Res 95:187–223

Pan Y (1997) Zircon and monazite forming metamorphic reactions at Manitouwadge, Ontario. Can Mineral 35:105–118

Parrish RR (1990) U–Pb dating of monazite and its application to geological problems. Can J Earth Sci 27:1431–1450

Percival JA, West GF (1994) The Kapuskasing Uplift; a geological and geophysical synthesis. Can J Earth Sci 31:1256–1286

Percival JA, Fountain DM, Salisbury MH (1992) Exposed crustal cross sections as windows on the lower crust. In: Fountain DM, Arculus R, Kay RW (eds) Continental lower crust. Elsevier, Amsterdam, pp 317–361

Peterson TD, van Breemen O, Sandeman HA, Cousens B (2002) Proterozoic (1.85–1.75 Ga) igneous suites of the western Churchill Province: granitoid and ultrapotassic magmatism in a reworked Archean hinterland. Precambrian Res 119:73–100

Pyle JM, Spear FS (1999) Yttrium zoning in garnet: coupling of major and accessory phases during metamorphic reactions. Geol Material Res 1(6):1–49

Rayner NM, Stern RA, Rainbird RH (2003) SHRIMP U–Pb detrital zircon geochronology of Athabasc Group sandstones, northern Saskatchewan and Alberta. Current Research 2003-F2:22 p

Ross GM, Eaton DW, Boerner DE, Miles W (2000) Tectonic entrapment and its role in the evolution of continental lithosphere: an example from the Precambrian of western Canada. Tectonics 19(1):116–134

Sanborn-Barrie M, Carr SD, Theriault R (2001) Geochronological constraints on metamorphism, magmatism and exhumation of deep-crustal rocks of the Kramanituar Complex, with implications for the Paleoproterozoic evolution of the Archean western Churchill Province, Canada. Contrib Mineral Petrol 141:592–612

Schoene RB, Crowley JL, Condon DJ, Schmitz MD, Bowring SA (2006) Reassessing the U and ^{40}K decay constants for geochronology: new insights from high-precision ID-TIMS U–Pb data. Geochim Cosmochim Acta 70:426–445

Snoeyenbos DR, Williams ML, Hanmer S (1995) An Archean eclogite facies terrane in the western Canadian Shield. Eur J Mineral 7:1251–1272

Spear FS, Pyle JM (2002) Apatite, monazite, and xenotime in metamorphic rocks. Rev Mineral Geochem 48:293–331

Stacey JC, Kramers JD (1975) Approximation of terrestrial lead isotope evolution by a two-stage model. Earth Planet Sci Lett 26:207–221

Stern RA, Berman RG (2000) Monazite U–Pb and Th–Pb geochronology by ion microprobe, with an application to in situ dating of an Archean metasedimentary rock. Chem Geol 172:113–130

Teyssier C (1985) A crustal thrust system in an intracratonic tectonic environment. J Struct Geol 7(6):689–700

Vance D, Muller W, Villa IM (2003) Geochronology: linking the isotopic record with petrology and textures—an introduction. Geol Soc Spec Pub 220:1–24

Williams ML, Hanmer S (2005) Structural and metamorphic processes in the lower crust: evidence from the East Athabasca mylonite triangle, Canada, a deep-crustal isobarically cooled terrane. In: Brown M, Rushmer T (eds) Evolution and differentiation of the Continental Crust. Cambridge University Press, Cambridge, pp 232–268

Williams ML, Jercinovic MJ (2002) Microprobe monazite geochronology: putting absolute time into microstructural analysis. J Struct Geol 24:1013–1028

Williams ML, Hanmer S, Kopf C, Darrach M (1995) Syntectonic generation and segregation of tonalitic melts from amphibolite dikes in the lower crust, Striding-Athabasca mylonite zone, Northern Sastachewan. J Geophys Res 100:15717–15734

Williams ML, Jercinovic MJ, Terry MP (1999) Age mapping and dating of monazite on the electron microprobe: deconvoluting multistage tectonic histories. Geology 27(11):1023–1026

Williams ML, Melis EA, Kopf C, Hanmer S (2000) Microstructural tectonometamorphic processes and the development of gneissic layering: a mechanism for metamorphic segregation. J Metamorph Geol 18:41–57

Williams ML, Jercinovic MJ, Goncalves P, Mahan KH (2006) Format and philosophy for collecting, compiling, and reporting microprobe monazite ages. Chem Geol 225:1–15

Wing BA, Ferry JM, Harrison TM (2003) Prograde destruction and formation of monazite and allanite during contact and regional metamorphism of pelites: petrology and geochronology. Contrib Mineral Petrol 145:228–250